Clim. Past Discuss., 9, 3125–3174, 2013
www.clim-past-discuss.net/9/3125/2013/
doi:10.5194/cpd-9-3125-2013

Climate of the Past Discussions
Open Access

Centennial-scale shifts in the position of the Southern Hemisphere westerly wind belt over the past millennium

B. G. Koffman[1,2,*], K. J. Kreutz[1,2], D. J. Breton[2,3,], E. J. Kane[1], D. A. Winski[1,2,***], S. D. Birkel[2], A. V. Kurbatov[1,2], and M. J. Handley[2]**

[1]School of Earth and Climate Sciences, University of Maine, 5790 Bryand Global Sciences Center, Orono, ME 04469, USA
[2]Climate Change Institute, University of Maine, 300 Bryand Global Sciences Center, Orono, ME 04469, USA
[3]Department of Physics and Astronomy, Bennett Hall, University of Maine, Orono, ME 04469, USA
[*]now at: Lamont-Doherty Earth Observatory of Columbia University, P.O. Box 1000, 61 Route 9W, Palisades NY, 10964, USA
[**]now at: Thayer School of Engineering, Dartmouth College, 14 Engineering Drive, Hanover, NH 03755, USA
[***]now at: Stantec Consulting Inc., 100 Pearl Street, 11th Floor, Hartford, CT 06103, USA

Received: 4 May 2013 – Accepted: 13 May 2013 – Published: 13 June 2013

Correspondence to: B. G. Koffman (bess.koffman@maine.edu)

Published by Copernicus Publications on behalf of the European Geosciences Union.

Abstract

We present the first high-resolution (sub-annual) dust particle dataset from West Antarctica, developed from the West Antarctic Ice Sheet (WAIS) Divide deep ice core (79.468° S, 112.086° W), and use it to reconstruct past atmospheric circulation. We find a background dust flux of ∼ 4 mg m^{-2} yr^{-1} and a mode particle size of 5–8 µm diameter. Through comparison with other Antarctic ice core particle records, we observe that coastal and lower-elevation sites have higher dust fluxes and coarser particle size distributions (PSDs) than sites on the East Antarctic plateau, suggesting input from local dust sources at lower elevations and sites closer to the coast. In order to explore the use of the WAIS Divide dust PSD as a proxy for past atmospheric circulation, we make quantitative comparisons between mid-latitude zonal wind speed and the dust size (coarse particle percentage, CPP) record, finding significant positive interannual relationships. Using our CPP record, and through comparison with spatially distributed climate reconstructions from the Southern Hemisphere (SH) middle and high latitudes, we infer latitudinal shifts in the position of the SH westerly wind belt during the Medieval Climate Anomaly (MCA; ∼ 950–1350 C.E.) and Little Ice Age (LIA; ∼ 1400–1850 C.E.) climate intervals. We suggest that the SH westerlies occupied a more southerly position during the MCA, and shifted equatorward at the onset of the LIA (∼ 1430 C.E.) due to cooler surface temperatures and a contraction of the SH Hadley cell.

1 Introduction

The Southern Hemisphere (SH) westerly winds (SWW) are a major driver of regional and global climate (Thompson and Solomon, 2002; Toggweiler et al., 2006). The SWW form a strong, zonally symmetric wind belt, centered at approximately 50° S, that circles the Antarctic continent (Fig. 1a). The SWW carry moisture, soil dust, volcanic ash, and other aerosols. A growing number of publications point to the SWW as the primary control on atmospheric CO_2 variability on glacial-interglacial timescales because

CPD
9, 3125–3174, 2013

wind stress on the Southern Ocean controls the rate of deepwater ventilation around Antarctica (Toggweiler et al., 2006; Anderson et al., 2009; Burke and Robinson, 2012). The Southern Ocean is the only region in the world's oceans where water of 2–3 km depth can upwell to the surface, coming into direct contact with the atmosphere (Russell et al., 2006). The rate of upwelling is governed by the strength of the Antarctic Circumpolar Current (ACC), which is driven by the SWW. The position of the SWW belt relative to the ACC determines the winds' influence on ventilation of these deep, CO_2-rich waters (Toggweiler, et al., 2006). During the last glacial termination, a climate modeling study suggests that a latitudinal shift of 3–4° toward Antarctica would significantly have increased the ventilation of deep water, resulting in CO_2-induced warming (Russell et al., 2006). A proposed mechanism for such shifts is that cold temperatures in the Northern Hemisphere (NH) push Earth's thermal equator southward, displacing the SWW poleward (Toggweiler et al., 2006; Denton et al., 2010). Such shifts in the SWW prior to climate warming events are corroborated by a new dust record from the EPICA Dome C ice core (East Antarctica; EPICA: European Project for Ice Coring in Antarctica). Sharp declines in dust deposition preceded changes in temperature during glacial terminations and Antarctic isotopic maxima over the past 800 000 yr, suggesting that rapid shifts in the SWW may have led to reductions in dust mobilization from Patagonian sources, while simultaneously increasing rates of deep ocean upwelling, leading to atmospheric warming (Lambert et al., 2012). Rapid changes in wind gustiness, driven by meridional temperature gradients, may also have affected dust mobilization (McGee et al., 2010). In addition, the SWW also are thought to play a major role in governing the rate of Agulhas leakage in the South Atlantic, thereby directly affecting the Atlantic Meridional Overturning Circulation (De Deckker et al., 2012). Therefore, through multiple mechanisms, the SWW exert a strong control on global climate.

The SWW also influence ocean-atmosphere CO_2 fluxes on shorter timescales (Takahashi et al., 2002). Indeed, changes in the position and strength of the SWW may be the main driver of CO_2 variability during the Holocene (Moreno et al., 2009, 2010). Although different proxies for SWW intensity and/or position yield potentially conflicting patterns

CPD
9, 3125–3174, 2013

of change during the early-to-mid-Holocene (Lamy et al., 2010; Bjorck et al., 2012), it seems apparent that the SWW shifted in response to larger-scale climate changes, most likely driven by changes in radiative forcing (Renssen et al., 2005; Varma et al., 2012). During the late Holocene, records from around the SH suggest a transition from zonally symmetric to zonally asymmetric patterns of SWW variability, a change attributed to increased high-frequency ENSO influence (Fletcher and Moreno, 2011, 2012a). Currently the SWW are intensifying and shifting poleward, largely due to the effect of stratospheric ozone depletion in the Antarctic region, with a lesser effect induced by greenhouse gas forcing (Thompson and Solomon, 2002; Arblaster and Meehl, 2006; Thompson et al., 2011; Lee et al., 2013). These changes in the winds have increased the ventilation rate of Southern Ocean waters in past decades, a trend that is likely to continue (Waugh et al., 2013). Enhanced upwelling of CO_2-rich deep waters has led to increased surface ocean CO_2 concentrations, while at the same time reducing anthropogenic carbon uptake (Lenton et al., 2009, 2012). Although ongoing changes in ozone and greenhouse gas concentrations are driving the SWW-Southern Ocean system into a non-analog state (Mayewski et al., 2009; Turner et al., 2009), it is important to understand how the SWW varied in strength and position in the past, in response to natural forcings. In particular, SWW variability on decadal to centennial timescales during the late Holocene remains poorly understood. What mechanisms cause the SWW to shift position and/or intensity? Do the winds respond to different forcings on different timescales? And how might these natural forcings change in response to ongoing anthropogenic warming?

Because of the dynamic response of dust emissions to climate forcing, high-resolution terrestrial dust archives, such as ice cores, can be used to understand the timing and mechanisms of past climate changes (Mayewski et al., 1994, 2009; Legrand and Mayewski, 1997). Ice core records have shown a tight, nonlinear coupling between dust flux and regional temperature on glacial/interglacial timescales (Steffensen, 1997; Petit et al., 1999; Wolff et al., 2006; Fischer et al., 2007; Lambert et al., 2008), a relationship that appears to have held over the past 4 million years (Martinez-Garcia et al.,

CPD
9, 3125–3174, 2013

2011). Observed changes in Antarctic dust flux have been linked to glacial activity (Sugden et al., 2009) and anthropogenic land-use changes (McConnell et al., 2007) in dust source regions, as well as to changes in atmospheric circulation and the intensity of the hydrological cycle (Petit et al., 1999; Fischer et al., 2007; Lambert et al., 2008, 2012; Mayewski et al., 2013). In addition, ice core records of aerosol iron deposition have been used to assess the potential impact of atmospheric dust on fertilizing the Southern Ocean (Edwards et al., 2006; Gaspari et al., 2006), the largest iron-limited region of the world oceans (Turner and Hunter, 2001). In addition to the information contained in dust flux records, particle size data can be used to understand the proximity of dust source(s) and the strength of atmospheric transport (e.g., Bory et al., 2010; Kok, 2011a). If the geographical source remains constant, the size distribution of particles can be used as an indicator of past changes in wind strength, providing valuable information that cannot be obtained through looking at chemical dust proxies (such as Al, Ce, and non-seasalt Ca, *nss*Ca) alone (Delmonte et al., 2002, 2005; Kok, 2011a).

Ice core records of dust (either microparticle or chemical dust proxy) deposition have been developed from a number of sites in Antarctica. Early ice coring efforts at Byrd Station, West Antarctica, provided the first view of large glacial/interglacial dust changes (Thompson, 1977), though at low temporal resolution. Deep ice cores from Vostok and Dome C in East Antarctica extended the Antarctic climate history to the past eight glacial cycles (Petit et al., 1999; Wolff et al., 2006; Lambert et al., 2008). Shorter time span but higher temporal resolution cores from coastal locations have provided insights into the seasonality of particle deposition (Ruth et al., 2004), the impact of human land-use changes on dust emissions (McConnell et al., 2007), and the variability of dust sources supplying different regions (Bory et al., 2010; Delmonte et al., 2010; Albani et al., 2012; Wegner et al., 2012). A suite of shallow ice cores obtained by the ITASE program has provided unprecedented spatial resolution for evaluating climate changes over recent centuries (ITASE: International Trans-Antarctic Scientific Expedition; Dixon et al., 2012). In addition, microparticle datasets exist from Siple Sta-

CPD
9, 3125–3174, 2013

tion, West Antarctica (Mosley-Thompson et al., 1990) and from a South Pole ice core (Mosley-Thompson and Thompson, 1982).

In this paper, we present results from microparticle analysis of the upper 577 m (2400 yr) of the West Antarctic Ice Sheet (WAIS) Divide deep ice core. The drill site is located roughly between the Antarctic Peninsula and the East Antarctic Ice Sheet (EAIS), in a high-accumulation area, allowing development of a continuous, highly temporally resolved dust deposition record ($\sim$ 10–20 samples yr^{-1}). We present dust flux, concentration, and size distribution records, and compare them to late Holocene data from other Antarctic ice cores. In addition, we present automatic weather station (AWS) and ERA-Interim reanalysis data in order to characterize local and regional-scale atmospheric circulation. We use correlations with reanalysis zonal wind speed to calibrate the dust record over the period 1979–2002, and argue that the coarse dust particle fraction is driven by variability in SWW intensity on an interannual basis.

A significant challenge in reconstructing past SWW behavior is to deconvolve changes in the latitudinal position of the SWW belt from independent changes in wind intensity. We believe that by synthesizing records spanning the latitudinal range of SWW influence, we can make progress toward this goal. Specifically, our aim is to understand how the latitudinal position of the SWW varied on decadal to centennial timescales during key intervals of climatic change in the late Holocene: the Medieval Climate Anomaly (MCA, $\sim$ 950–1350 C.E.) and the Little Ice Age (LIA; $\sim$ 1400–1850 C.E.). We use our coarse particle record in conjunction with paleohydrological reconstructions from the SH mid-latitudes to suggest that the SWW occupied a more southerly position during the MCA, and shifted to a more northerly position during the LIA.

CPD
9, 3125–3174, 2013

2 Methods

2.1 WAIS Divide ice core melting and analysis

The West Antarctic Ice Sheet (WAIS) Divide ice core was drilled to a depth of 3405 m in central West Antarctica (79.468° S, 112.086° W; 1766 m a.s.l.; Fig. 1). The average accumulation rate of 0.207 m_{weq} yr^{-1} (Banta et al., 2008) is sufficient for detection of well-preserved annual layers well below the depths analyzed here. We melted the upper 577 m of the deep ice core, WDC06A, using a continuous ice core melting system with both continuous flow-through analysis (CFA) and discrete sampling for geochemical and microparticle analysis (Breton et al., 2012). Prior to melting, core ends and breaks were scraped under a HEPA hood using a clean ceramic blade to reduce possible contamination from drilling fluid and other sources. Despite this mechanical cleaning, we observed that core breaks tended to introduce particulate contamination into the ice. Therefore, during our data processing procedure, we removed dust concentration peaks that were associated with observed breaks in the ice core.

The ice core meltwater was analyzed for microparticle concentrations using a CFA laser particle detector (LPD; Klotz Abakus), and for electrolytic conductivity using a CFA conductivity cell (Amber Science). Depth co-registration for both datasets was achieved using a weight and rotary encoder and our sample-tracking algorithm, achieving a depth uncertainty of ±1 mm. The effective depth resolution obtained by our system, limited by signal dispersion, is 1.0 cm in glacial ice and ∼ 2 cm in low-density firn, which is equivalent to ∼ 10–20 samples yr^{-1} for the late Holocene core analyzed here (Breton et al., 2012). Raw time series data were filtered using a low-pass filter based on the PL64 filter, with a time step of 1.64 days and a cutoff of either 12 or 252 months (1 or 21 yr; G. Gerbi, personal communication, 2011).

Using the LPD, we analyzed insoluble particles in 31 size channels, spanning 1.0 to 15.0 µm diameter, and calculated particle concentrations using directly measured flow rates. The LPD was calibrated with Antarctic snow samples using a Coulter Counter, as described by Ruth et al. (2003). By calibrating the instrument using environmental

CPD
9, 3125–3174, 2013

samples (rather than latex standards), we attempted to avoid some of the size calibration issues described by Lambert et al. (2012), namely, that spherical particles are a poor proxy for the range of shapes exhibited by insoluble dust particles. After calibration, we tested the Abakus using commercial size and concentration standards, and found that it accurately measured latex spheres of 1, 2, 5 and 10 µm diameter and successfully registered the orders-of-magnitude differences in concentration that we tested (not shown). In addition, we melted and analyzed six pairs of replicate ice "sticks" cut parallel from the same one-meter section of ice core. We melted these "sticks" in antiparallel orientations to evaluate signal fidelity measured using our CFA instruments. Results from replicate core analysis show excellent reproducibility in both signal depth and magnitude (see Fig. 7 in Breton et al., 2012). Particle size distributions (PSDs) were determined by calculating the total volume of mineral dust contained within each size bin, assuming spherical dimensions, and then taking the derivative of the particle volume with respect to the derivative of the natural logarithm of the particle diameter for each bin ($dV/d\ln D$ in $\mu m^3\,mL^{-1}$). We use the mode particle diameter µ as a descriptive statistic for the center of the volume size distribution, following Ruth et al. (2003).

We applied the WDC06A-7 timescale, which is based on annual layer counting of chemical signals in the ice core. The timescale has an estimated age uncertainty of ±1 yr for the depth range 0–577 m, analyzed here (WAIS Divide Project Members, 2013). Annually resolved accumulation rates were calculated for the WAIS Divide core by using the depth-age relationship and applying a one-dimensional ice-flow model, as described by WAIS Divide Project Members (2013). To calculate dust flux, we applied these accumulation rates assuming 0.5 basal sliding fraction; different basal sliding fractions do not make a significant difference in the calculated accumulation rates during the Holocene (WAIS Divide Project Members, 2013).

2.2 Automatic weather station data

We obtained automatic weather station (AWS) data from the Antarctic Meteorological Research Center and Automatic Weather Stations Project server at the Space Science

CPD
9, 3125–3174, 2013

and Engineering Center, University of Wisconsin (Lazzara et al., 2012). We used wind speed and direction data, which were collected nominally every ten minutes, although there were numerous instrument failures that caused gaps in data. Data were subjected to basic quality control prior to being archived; we removed data with zero values for both wind speed and direction, as these occurred over long spans of time, intermingled with data gaps, and appeared to be errors. Measurements span 2009–2012 for the WAIS Divide Field Camp AWS, named Kominko–Slade. For the months with archived data, we estimated the percentage of actual data measurements vs. data gaps for each season: DJF 90 %, MAM 82 %, JJA 37 %, and SON 47 %. As might be expected, the AWS functioned best in summer (DJF) and worst in winter (JJA). Even with the low data-recording rates during winter and spring, we believe these data provide a useful picture of general wind conditions at the WAIS Divide site that can be compared with reanalysis surface wind data.

2.3 Reanalysis data

We obtained ERA-Interim full resolution, six-hour daily field reanalysis data (76 km resolution) from the European Centre for Medium-Range Weather Forecasts research data server (Dee et al., 2011). From the 10 m U (zonal) and V (meridional) wind components, we calculated wind speed (W_{spd}) and direction (W_{dir}) using the following equations (from www.eol.ucar.edu), which allowed us to compare reanalysis data directly to the AWS surface wind data.

$$W_{spd} = \sqrt{U^2 + V^2} \quad (1)$$

$$W_{dir} = \tan^{-1}(-U, -V) \cdot 180/\pi \quad (2)$$

Because the AWS data from WAIS Divide only span 2009–2012, we used this time period for comparison with the 10 m wind speed and direction data. We used seasonal and annual mean 700 hPa and 850 hPa U wind speed data to evaluate relationships between larger-scale circulation and our dust record. Spatial correlation maps show

CPD
9, 3125–3174, 2013

Pearson's linear correlations between zonal wind speed at each reanalysis grid point and the WAIS Divide dust record for the period of overlap, 1979–2002.

3 Results

3.1 Dust concentration, flux, and size distribution

Dust flux varied between ~2 and 25 mg m^{-2} yr^{-1} for most of the past 2400 yr, remaining typically around 3–5 mg m^{-2} yr^{-1}. Dust mass concentration was typically ~ 10–15 µg kg^{-1}. The two records exhibit very similar patterns, suggesting that changes in mass concentration drive observed changes in flux (Fig. 2c, d). In other words, because the snow accumulation rate at WAIS Divide has been relatively constant during the late Holocene, it appears to have had little to no influence on the dust concentration or flux (Fig. 3). Considering the lack of relationship seen between dust concentration and accumulation rate (linear regression slope = 2.5; r = 0.01), we infer that wet deposition dominates at this site. In contrast, if we saw a negative relationship between accumulation rate and dust concentration, we would infer a primarily dry dust deposition mechanism (Kreutz et al., 2000a). Because the dust mass concentration and flux records are consistent, and because published dust flux values can be compared readily among sites with different snow accumulation rates (e.g., Wolff et al., 2006), we use dust flux as a measure of dust deposition for comparison with other records.

There are four intervals during which dust flux increases dramatically from background levels of ~ 4 mg m^{-2} yr^{-1} to peaks near 10–25 mg m^{-2} yr^{-1}: ~ 122–90 B.C.E., ~ 156–195 C.E., ~ 1230–1440 C.E., and ~ 1850–2002 C.E. Because dust flux can be driven independently by changes in the number of particles deposited (i.e., dust particle number concentration) or by changes in the size distribution of those particles, we compare these three parameters. We use the coarse particle percentage (CPP; defined as number of particles mL^{-1} [4.5–15]/[1–15] µm diameter ×100) as a measure of the size distribution. From Fig. 2 we can see that the first two events are clearly

CPD
9, 3125–3174, 2013

visible in the number concentration data (Fig. 2a), but not present in the CPP record (Fig. 2b). In contrast, the major event at ~ 1230–1440 C.E. is present in all three parameters, but the structure and timing of changes is slightly different among them. The CPP begins to increase around the year 1050 C.E., and ramps up slowly to a maximum of 9.9 ± 2.7 % at ~ 1300 C.E. It remains elevated until a rapid drop to 3.7 ± 1.1 % at ~ 1430 C.E., followed by a second, smaller peak (5.1 ± 2.2 %) spanning the period ~ 1510–1610 C.E. During the period from 1610–1960 C.E., the CPP remains relatively low, at 3.5 ± 1.1 %. The dust number concentration shows a bimodal peak, with a maximum of 900 ± 590 particles mL^{-1} reached at ~ 1300 C.E., followed by a series of smaller peaks leading up to an increase beginning ~ 1820 C.E. The fourth interval with elevated dust flux, from ~ 1850 C.E. to the present, is characterized by a large increase in the dust number concentration (from 220 ± 120 particles mL^{-1} during the decade 1850–1860 to 860 ± 370 particles mL^{-1} during the decade 1990–2002), but relatively little change in the CPP until much later, ~ 1960 C.E. The CPP averages 4.8 ± 0.9 % during the last decade of the record (1990–2002), and appears to be following an increasing trend.

In summary, we observe three patterns of behavior among the dust number concentration, the dust flux, and the CPP: (1) synchronous increases in the dust number concentration and flux records during ~ 122–90 B.C.E. and ~ 156–195 C.E. with negligible change in the CPP; (2) a simultaneous peak in all three parameters at ~ 1300 C.E. but with different structures between the records; and (3) roughly synchronous increases in concentration and flux beginning in the mid-1800s and peaking at the present, with a later and smaller-amplitude change in the CPP during recent decades.

Although we primarily use the CPP as a measure of changes in PSD, the volume size distribution $dV/d\ln D$ provides additional information about dust source and transport. We can use both the shape of the distribution (Kok, 2011a, b) and its relative mode (Bory et al., 2010; Delmonte et al., 2010) to infer proximity to dust source, and can use changes in mode size to infer variability in transport strength (Delmonte et al., 2005; Ding et al., 2002; Ruth et al., 2003). We find that the background dust (i.e., non-volcanic) PSD has a mode diameter that varies between ~ 5–8 µm (Fig. 4). We selected

CPD
9, 3125–3174, 2013

three representative time intervals to include in Fig. 4, to demonstrate how the volume size distribution relates to the CPP: 1250–1300 C.E. (high CPP, mode 7.2 µm), 1680–1730 C.E. (low CPP, mode 5.1 µm), and 1960–2002 C.E. (high CPP, mode 5.1 µm but with greater contribution from coarse particles compared to the LIA interval). We find that the modern PSD approaches the MCA PSD, consistent with recently observed changes in the SWW and with our hypothesis that particle size changes at WAIS Divide are driven by changes in the westerlies. Figure 4 also shows the theoretical dust volume size distribution at emission, which is based on evidence that dust emission is a scale-invariant process (Kok, 2011b). In other words, the emitted dust PSD depends on the source soil PSD, and not on the wind speed at the emission site (Kok, 2011a, b). The shape of the WAIS Divide volume size distribution approaches that of the theoretical emission size distribution, suggesting that while the dust must be transported some distance from its source, it is not travelling as far as the Patagonian dust reaching East Antarctic ice core sites, which has a lognormal or Weibull distribution (Delmonte et al., 2002). It appears that while we captured the center (mode) of the distribution, we did not observe the entire size distribution of particles deposited at WAIS Divide because of our analytical limit of 15 µm diameter. Future work in central West Antarctica should strive to analyze particles in a larger size range (e.g., up to 30 µm diameter) in order to determine the nature of the size distribution, and whether it is unimodal or polymodal.

3.2 Regional wind characteristics

Both AWS data and ERA-Interim reanalysis data from the WAIS Divide site illustrate seasonal patterns in local wind speed and direction (Fig. 5). We observe a consistent pattern of onshore winds, with the predominant surface wind direction being approximately from the northeast. The two datasets agree well, although the ERA-Interim summer (DJF) winds show a stronger easterly component than do the AWS summer winds. Winds of all recorded speeds come from this dominant direction; in other words, there is no pattern of stronger winds coming from one direction, and weaker winds coming from another. However, we do observe seasonal patterns in wind strength: winter

CPD
9, 3125–3174, 2013

(JJA) wind data have the greatest percentage of recorded wind speeds over 15 m s^{-1} and summer wind data have the lowest. The patterns in the reanalysis data are verified by the instrumental record. Because the data recording frequency is every 10 min for the AWS data and every 6 h for the ERA-Interim data, we suspect that high wind speed events will be recorded more frequently in the observational record, which appears to be the case.

3.3 Relationship between winds and coarse particle percentage

We see a significant positive correlation ($r = 0.3$–0.5, $p < 0.1$) between the annual mean mid-latitude westerly zonal (U) wind speed and the annual mean CPP at both 700 hPa (Fig. 6) and 850 hPa (not shown). Looking at the correlations between annual mean CPP and seasonal mean zonal wind speed for each season, we see some variability in the longitudinal regions of highest correlation (Fig. 7). During summer (DJF) and fall (MAM), the CPP is significantly correlated ($r = 0.3$–0.5, $p < 0.1$) with zonal winds in much of the SWW belt (Fig. 7a, b). In contrast, the winter (JJA) and spring (SON) correlation maps show greater zonal "patchiness" (Fig. 7c, d). In winter, the region of strongest correlation ($r = 0.4$–0.5, $p < 0.1$) spans the region from Queen Mary Land to Marie Byrd Land ($\sim 100^{\circ}$ E to $\sim 150^{\circ}$ W), to the west of the Amundsen–Bellingshausen Sea region. In spring, the region of strongest correlation ($r = 0.3$–0.5, $p < 0.1$) spans the region offshore from Victoria Land to the Amundsen Sea ($\sim 180^{\circ}$ W to $\sim 120^{\circ}$ W). We suspect these zonal differences may relate to zonal differences in the relative strength of winds in different seasons, likely driven by changes in the position of the Amundsen Sea Low pressure center (Kreutz et al., 1997, 2000b). Another possibility is that the stronger summer correlation reflects a real difference in SWW position, as the wind belt is located farther to the south in summer (Lamy et al., 2010).

CPD
9, 3125–3174, 2013

4 Discussion

4.1 Grain size distribution and likely dust source(s) for West Antarctica

Our measured PSD, with a mode size around 5–8 µm, is comparable to those measured at other non-EAIS plateau sites, including Talos Dome (2315 m a.s.l.) and Berkner Island (899 m.a.s.l.). Bory et al. (2010) found a substantial contribution of dust mass from > 5 µm diameter particles in surface snow at Berkner Island (a mode size was not reported). Using Sr and Nd isotopic data in conjunction with grain size measurements, they inferred the presence of an Antarctic dust source, in addition to a Patagonian dust source, with different sources predominating in different seasons (Bory et al., 2010). Similarly, the Holocene section of the Talos Dome ice core dust record is dominated by particles in the 5–10 µm diameter range, suggesting proximal dust sources (Albani et al., 2012). Delmonte et al. (2010) investigated dust provenance using Sr and Nd isotopes, and found that the Holocene dust signature matches nearby sources in the Transantarctic Mountains. In contrast, during glacial times, the Talos Dome dust PSD approximated a lognormal distribution with a mode size around 2 µm diameter (Albani et al., 2012), and the isotopic signature reflected dust input primarily from Patagonia (Delmonte et al., 2010); local dust sources may have been covered by permanent snow or ice at this time (Albani et al., 2012). Holocene dust sizes measured at these sites are all relatively coarse compared to the ∼ 2 µm modal values measured in the Vostok and EPICA Dome C ice cores from central East Antarctica (e.g., Delmonte et al., 2002). According to a range of geochemical and isotopic evidence, the East Antarctic plateau receives dust primarily from Patagonia, located approximately 6–7000 km distant, although other sources, such as Australia, may contribute during interglacial periods (Basile et al., 1997; Delmonte et al., 2004, 2008; Marino et al., 2008, 2009). Given the particle size similarities between WAIS Divide and other non-plateau sites, it seems plausible that much of Antarctica has a dust size signature that differs from that of central East Antarctica. Coarser PSDs likely indicate shorter dust transport distances and may imply a predominance of local (Antarctic) sources.

CPD
9, 3125–3174, 2013

Observed differences in grain size distributions between East Antarctic plateau sites (~ 3200–3500 m.a.s.l.) and lower-elevation sites such as Berkner Island, Talos Dome, and WAIS Divide may also indicate differences in the transport altitude of atmospheric dust, as suggested by Bory et al. (2010). While dust from the major Southern Hemisphere dust sources, Patagonia and Australia, is transported at altitudes of > 4000 m (Li et al., 2008; Krinner et al., 2010), it is possible that dust from Antarctic sources, which are poorly characterized, may travel too low in the troposphere to reach the East Antarctic plateau. A possible analog occurs in Asia, where Wu et al. (2009) found a negative correlation between glacier elevation and particle size in ice core samples from the Tibetan Plateau, consistent with the observed Antarctic pattern. Particles in cores from the Muztagata glacier at 6250 and 6350 m a.s.l. had mean mode sizes of 5.87 and 5.74 µm, respectively, coarser than the mean mode size of 4.99 µm measured at 7010 m a.s.l.; PSDs at the higher elevation site were also less variable (Wu et al., 2009). Thus, we interpret the observed decrease in grain size with elevation to reflect decreasing influence of local dust emissions.

In addition to particle size information, the general shape of a dust PSD can be used to infer transport distance (Kok, 2011a). The WAIS Divide PSD differs from the PSDs of dust from Greenland (Steffensen, 1997; Ruth et al., 2003) and central East Antarctica (Delmonte et al., 2002), which are lognormal. Instead, it falls somewhere between a lognormal distribution and a distribution of dust particles near their emission source (Fig. 4; Kok, 2011a). Considering both the coarser mode size compared to central EAIS dust and the shape of the distribution, we infer a relatively shorter dust transport distance in central WAIS compared to the EAIS plateau.

Given the dominant wind direction from the Amundsen–Bellingshausen Sea region to the WAIS Divide site (Fig. 5), we believe that potential nearby dust sources would have to be located in coastal Marie Byrd Land. We suggest that the consistency of wind direction from this coastal region during all seasons makes dust contributions from sites in the Transantarctic Mountains, Ellsworth Mountains, or other nunataks located to the south and west unlikely. Modeling studies suggest either a predominance of Australian

CPD
9, 3125–3174, 2013

dust or a roughly 50–50 mixture of South American and Australian-sourced dust to the WAIS at present (Li et al., 2008; Albani et al., 2011). However, to our knowledge, no studies have yet evaluated the possible role of dust from other sources, such as New Zealand or the particularly dusty Dry Valleys west of McMurdo Sound, Antarctica. Reanalysis wind data show that the McMurdo Sound region is dominated by southerly flow (Fig. 1b), suggesting that dust from the Dry Valleys could enter the southern margin of the SWW belt and be transported to WAIS Divide. Additional work will be needed to assess the extent, emissions activity, and geochemical signature of Antarctic potential dust source areas.

4.2 Flux comparison to other sites

The WAIS Divide late Holocene background (i.e., non-volcanogenic) dust flux of $\sim 4\,\mathrm{mg\,m^{-2}\,yr^{-1}}$ appears to be intermediate between coastal sites in the Weddell Sea region and sites located on the East Antarctic plateau. A factor of ~ 3 higher dust flux ($12\,\mathrm{mg\,m^{-2}\,yr^{-1}}$) was reported for the mid-to-late 19th century at James Ross Island, near the tip of the Antarctic Peninsula and close to Patagonian dust sources (McConnell et al., 2007). Similarly, although flux values have not been reported for the Berkner Island ice cores, the average dust concentration of 1220 ± 1110 particles $\mathrm{mL^{-1}}$ is 5 times that observed at WAIS Divide (230 ± 350 particles $\mathrm{mL^{-1}}$) for the same time period (1080–1994 C.E.), while the accumulation rate is $\sim 60\,\%$ lower (average: $130\,\mathrm{kg\,m^{-2}\,yr^{-1}}$ vs. $207\,\mathrm{kg\,m^{-2}\,yr^{-1}}$ at WAIS Divide; Ruth et al., 2004; Banta et al., 2008). Given the predominance of particles in the 5–10 µm diameter range at Berkner, we suggest that the dust mass flux is likely greater than at WAIS Divide. In addition, Bory et al. (2010) report that the dust flux measured at Berkner Island is similar to that measured at Kohnen Station, Dronning Maud Land (2892 m a.s.l.) for small (< 3 µm diameter) particles, but is up to 3.5 times higher for particles in the 3–9 µm diameter range. This observation is consistent with the idea that coastal and lower-elevation sites display a coarser dust size distribution than sites at higher elevations, perhaps due to local dust source activity (Bertler et al., 2005). On the eastern margin of the EAIS, the

CPD
9, 3125–3174, 2013

late Holocene dust flux at Talos Dome was ~ 1 mg m^{-2} yr^{-1} for particles of 1–10 µm diameter (Albani et al., 2012). In contrast to these coastal and lower-elevation sites, the interglacial dust flux reported from the EPICA Dome C ice core, 0.2–0.6 mg m^{-2} yr^{-1}, is about an order of magnitude lower (Lambert et al., 2012).

Overall, these observations imply a meridional gradient in dust flux, as suggested by Edwards et al. (2006), based on atmospheric iron flux measurements from the Law Dome and EPICA Dome C ice cores. Because dust volume (and therefore mass) scales with the cube of the particle radius, we suggest that differences in particle size (rather than number) drive this flux gradient. This argument lends additional support to the idea that non-glaciated areas along the margins of the Antarctic ice sheets contribute a substantial amount of dust to the atmospheric dust burden over Antarctica, at least below ~ 3000 m, and implies that this locally sourced dust may also play a role in fertilizing the Southern Ocean.

4.3 Dust concentration, flux, and size distribution changes

We interpret changes in dust flux that are not accompanied by an increase in coarse particle deposition to indicate past changes within the dust source region(s). There are three intervals where we see significant increases in flux without a concomitant increase in CPP: ~ 122–90 B.C.E., ~ 156–195 C.E., and ~ 1850–2002 C.E. We attribute these increases to changes in the dust source strength. Such changes could be caused by availability of material, for example due to glacier activity (e.g., Sugden et al., 2009) or desertification (e.g., McConnell et al., 2007), or could be caused by a shift in the wind patterns in the dust source region (e.g., Lambert et al., 2012). We think that the increase in dust flux observed over the past 150 yr is due in part to human activity, likely in Australia (Li et al., 2008), while earlier dust flux changes probably were climatically driven. We focus now on interpreting the observed changes in dust CPP.

There are several possible interpretations for observed coarsening of the dust PSD: (1) a change from a more distal to a more proximal dust source; (2) a shift toward

CPD
9, 3125–3174, 2013

coarser particles at the emission site; and (3) increased transport efficiency, either through a change in circulation patterns or through increased wind strength. The first possible interpretation would require the activation of a local (i.e., Antarctic) dust source (or sources) during the time interval of observed increased CPP (~ 1050–1430 C.E.), followed by an abrupt deactivation. In this case, we would expect mixing of dust from two source regions, one distal, such as Australia, and the other proximal, with the latter contributing varying fractions of the total dust through time. Considering that the availability of sediment from such a local source would most likely be controlled by snow accumulation, we can use West Antarctic snow accumulation rates to argue against this interpretation. In addition to the annual accumulation rates from the WAIS Divide deep ice core (Fig. 2e; WAIS Divide Project Members, 2013), Banta et al. (2008) calculated accumulation rates for three ice cores from the WAIS Divide region: ITASE 00–1, WDC05A, and WDC05Q. While these records do not extend earlier than the year 1521 C.E., they provide an estimate of spatial variability in snow accumulation rate and can be used to compare to the past few centuries' dust PSD. Accumulation rates at all four sites remained relatively constant during the late Holocene, suggesting that changes in regional precipitation were unlikely to have driven the observed shifts in PSD. Further, if local sources were responding to changes in regional precipitation, we would expect to see an inverse relationship between dust flux and accumulation rate; however, we see no relationship (linear regression slope = −0.28; $r = 0$; Fig. 3). Moreover, the relatively constant snow accumulation rate and lack of relationship between accumulation and dust mass concentration argue against significant changes in atmospheric moisture content, which could affect rates of particle aggregation during transport and therefore our dust size distribution record.

The second possible interpretation, of a shift in the dust PSD at the emission site, seems unlikely given typically slow changes in soil grain size, and recent work showing that the dust size distribution at emission is independent of wind speed (Kok, 2011a). Contrary to conventional wisdom, Kok (2011a) showed through a compilation of field measurements that dust PSD does not vary with surface wind stress. Assuming a con-

CPD
9, 3125–3174, 2013

stant soil/sediment PSD at the source, which determines the dust size at emission (Kok, 2011b), this suggests that observed increases in mean particle size in terrestrial dust archives reflect either a more proximal source, or stronger transporting winds (Kok, 2011a).

Based on these arguments and on the significant positive correlations we observe between the CPP and zonal wind speed, we interpret the observed changes in dust PSD to represent wind strength variability. While the coarseness of the PSD in West Antarctica (in both Byrd and WAIS Divide ice cores) may indicate the presence of a local source, we do not find evidence for the turning off and on of such a possible source. Rather, we suggest that the sources themselves remained constant and that our observed PSD changes reflect changes in the winds transporting the dust.

Nicolas and Bromwich (2011) note that Marie Byrd Land is the only region in Antarctica where mean katabatic flow has a strong southward component, effectively resulting in parallel surface and 700 hPa flow, as is evident in our comparison of 10 m and higher-altitude wind data (e.g., compare wind directions in Figs. 1b and 5). Because of the unusual relationship between surface and middle troposphere winds in this region, we suggest that central West Antarctica is a site well-suited to paleowind reconstruction. The significant correlations we find between mid-latitude zonal wind speed and the CPP support wind strength as the driving cause of the observed changes in dust particle size. Our interpretation linking local wind speed to larger-scale circulation is consistent with recent analyses of zonal wind speed and cyclogenesis in the Amundsen–Bellingshausen Sea region. Lubin et al. (2008) found that during positive Southern Annular Mode (SAM) polarity, zonal wind speed intensifies and winter-spring cyclogenesis increases. We suspect that the frequency and intensity of cyclones in this region is a key driver of changes in dust PSD, and that when the SWW shift equatorward, the WAIS Divide site is less influenced by these cyclones. Thus, we can use our record in conjunction with others spanning the mid- to high southern latitudes to develop a hypothesis for past westerly wind behavior.

CPD
9, 3125–3174, 2013

Previous studies have linked westerly wind strength with WAIS dust deposition, using the crustal dust tracer *nss*Ca. Yan et al. (2005) found significant positive correlations between the mid-latitude zonal winds and *nss*Ca concentrations in the Siple Dome (coastal WAIS) and ITASE 00-1 (central WAIS) ice cores during recent decades. Dixon et al. (2012) expanded this work by using stacked *nss*Ca concentrations from ten ice cores to develop a proxy for northerly air mass incursions (NAMI) into central West Antarctica. They observe an increasing trend in *nss*Ca concentrations beginning around 1960 C.E., the same year we see the CPP at WAIS Divide begin to increase. Given a demonstrated relationship between *nss*Ca and insoluble particles (Ruth et al., 2008; Lambert et al., 2012), the similarities between these records make sense. However, a microparticle record contains independent information on environmental/dust source changes and transport changes, whereas *nss*Ca concentrations reflect the combined influence of particle size and number, effectively giving a combined signal of source and transport effects. Therefore, we suggest that the dust PSD provides a more robust tool for investigating the strength of the circum-Antarctic atmospheric circulation in the pre-instrumental era, as it is based on a physical relationship between wind strength and particle size.

4.4 Paleoclimatic interpretation

Given the demonstrated relationship between regional atmospheric circulation strength and the CPP record from WAIS Divide, we interpret the CPP record in terms of variability in the SWW. The major features of our record roughly coincide with the NH MCA and LIA climate intervals, the most dramatic climate changes of the late Holocene (O'Brien et al., 1995; Stuiver et al., 1995). We infer stronger SWW and/or a more poleward position from ~ 1050–1430 C.E., and weaker SWW and/or a more equatorward position from ~ 1430–1950 C.E. (with a minor strengthening or poleward shift from ~ 1510–1610 C.E.). In recent decades, we see an increase in the CPP, consistent with observations that the SWW have been strengthening and moving southward (Thompson and Solomon, 2002). Prior to ~ 1050 C.E., our record indicates variability in the SWW, with

CPD
9, 3125–3174, 2013

several short intervals of enhanced strength and/or more southerly position at ~ 400–264 B.C.E., 84–160 C.E., and 255–345 C.E. Although we cannot obtain information on SWW latitudinal position from one site alone, we can use our record in conjunction with climate reconstructions from the SH mid-to-high latitudes to develop a hypothesis for how the SWW belt has changed in latitudinal position through time. Through comparison to these records, we suggest that variability in the CPP is driven not only by changes in SWW intensity, but also by the relative position of the SWW belt (Fig. 8). Figure 9 summarizes our interpretations of past changes in SWW position, based on our CPP and hydrological reconstructions from the mid-latitudes.

Because the SWW are the primary driver of rainfall variability in the SH mid-latitudes (Fletcher and Moreno, 2011), a range of tools have been used to infer past changes in moisture balance (precipitation minus evaporation, P – E), and therefore variability in the SWW. Records from Patagonia provide a consistent picture of hydrologic change over the past millennium, with warmer/drier conditions during the MCA and cooler/wetter conditions during the LIA. Fletcher and Moreno (2012b) used pollen and charcoal particles in a sediment core from Laguna San Pedro (~ 38° S) to reconstruct climate and fire regime over the past 1500 yr. They found evidence of warmer and drier conditions, including enhanced charcoal deposition and predominance of *Poaceae* (grass) pollen, during the period ~ 1050–1400 C.E., and of cooler and moister conditions during LIA time, indicated by an increase of *Nothofagus* (southern beech) pollen (Fig. 8b; Fletcher and Moreno, 2012b). Lamy et al. (2001) used the iron concentration record from marine sediment core GeoB 3313–1 (~ 41° S) as a proxy for the rainfall history of southern Chile. Based on changes in terrigenous sediment composition linked to coastal vs. Andean source regions, they inferred drier conditions and a poleward shift of the SWW during the MCA followed by increased rainfall and an equatorward shift of the SWW during the LIA. Farther south, Moy et al. (2008) used pollen and *Pisidium* bivalve $\delta^{18}O$ measurements to infer changes in evaporation and precipitation in the region of Lago Guanaco, SW Patagonia, Chile (~ 52° S; Fig. 8c). Their record indicates increased aridity due to warmer summer temperatures from ~ 1050–1250 C.E.,

CPD
9, 3125–3174, 2013

indicated by enhanced *Poaceae* pollen and higher $\delta^{18}O$ values. During ~ 1500–1800 C.E., Moy et al. infer stronger wind-driven evaporation as well as increased precipitation (during different seasons), as indicated by a coincident increase in *Nothofagus* pollen and $\delta^{18}O_{Pisidium}$. Although they interpreted these changes as being consistent with a strengthening and poleward shift in the SWW during the LIA, we suggest, given the increased precipitation inferred farther to the north (Lamy et al., 2001; Fletcher and Moreno, 2012b) and the decreased CPP at WAIS Divide, that these changes may have been caused by a northerly shift of the SWW.

Evidence from a lake record in South Africa is consistent with the timing and direction of changes observed in Patagonia during MCA and LIA times. Using a sediment core from Lake Verlorenvlei (~ 32° S), Stager et al. (2012) found evidence of more arid conditions during the MCA and of increasing P–E and runoff since ~ 1400 C.E. They inferred a strengthening and/or northward shift of the SWW around 1400 C.E.

Records from Australia and New Zealand tend to show patterns of past precipitation change that are neither consistently in-phase nor out-of-phase with those in the eastern Pacific. In Tasmania, a sediment record developed from Rebecca Lagoon (~ 41° S) shows evidence of enhanced precipitation from ~ 1000–1500 C.E. and ~ 1650–1850 C.E., with a drier interval in between (Saunders et al., 2012). Fjord sediment core records from southern South Island, New Zealand (44.5°–46.5° S) indicate generally drier conditions during periods with cooler temperatures, at ~ 550–950 C.E. and ~ 1200–1800 C.E., with a wetter interval from ~ 950–1200 C.E. (Knudson et al., 2011). Knudson et al. (2011) found no clear relationship between Fiordland records and Patagonian precipitation reconstructions from similar latitudes, and suggested that in addition to potential changes in the extent and intensity of the SWW belt, the SWW varied zonally, likely due to interactions with atmospheric pressure systems which shift in response to changes in high-frequency climate oscillations such as the Southern Annular Mode (SAM) and ENSO (Knudson et al., 2011; Southern Oscillation Index proxy reconstruction from Yan et al. (2011) shown for reference in Fig. 8a).

CPD
9, 3125–3174, 2013

Other high-resolution ice core records from Antarctica also have been used to infer past changes in atmospheric circulation. Sea-salt sodium (*ss*Na) concentrations in the Siple Dome, West Antarctica, ice core have been interpreted as a proxy for the Amundsen Sea Low (ASL), a persistent feature of the circum-Antarctic atmospheric circulation (Kreutz et al., 1997, 2000b; Maasch et al., 2005). The Law Dome, East Antarctica, ice core *ss*Na record has been used to reconstruct variability in the SAM, based on a statistical relationship between early winter seasonal *ss*Na concentrations and mean sea-level pressure (Goodwin et al., 2004; Vance et al., 2013). In both cases, enhanced *ss*Na deposition has been interpreted as an indicator of increased meridional transport from the ocean to the ice core site. However, *ss*Na is also produced during the formation of frost flowers as sea ice freezes (Wagenbach et al., 1998; Rankin et al., 2000). Several studies have shown that *ss*Na is an effective proxy for sea ice extent, particularly at Antarctic coastal sites, suggesting that its variability is not driven by enhanced storminess (Rankin et al., 2002; Wolff et al., 2003, 2006). Because *ss*Na deposition may be influenced by multiple factors, we do not attempt to relate observed changes in the Siple and Law Dome ice core *ss*Na records to those we describe in the WAIS Divide microparticle record.

In summary, it seems evident that paleoclimate reconstructions from the SH mid-to-high latitudes indicate not only changes in the intensity of the SWW, but also shifts in the position of the wind belt. Given evidence from terrestrial and marine records spanning 32° S to 52° S, we infer that the SWW occupied a more southerly position during the period ~ 1050–1430 C.E., and shifted to a more northerly position at ~ 1450 C.E., remaining there until around 1850–1950 C.E. During the last ~ 40 yr of the record (1960–2002), increasing coarse particle deposition is consistent with observations that the SWW have been shifting southward and intensifying (Thompson and Solomon, 2002).

If we extend our analysis to the past two millennia, we can explore the relationship between ENSO and the inferred shifts in SWW position. The precipitation-based proxy for the Southern Oscillation Index (SOI_{pr}) developed by Yan et al. (2011) indi-

CPD
9, 3125–3174, 2013

cates predominant El Niño-like conditions during the MCA, and La Niña-like conditions during the LIA. Although this model of ENSO state contrasts with SST-based reconstructions (e.g., Cobb et al., 2003), it is consistent with the Laguna Pallcacocha record of El Niño-driven erosion events developed from Ecuador (Moy et al., 2002). The Lamy et al. (2001) precipitation-driven iron record, from the northern margin of SWW influence, shows close agreement with the SOI_{pr} reconstruction. Our CPP record, much to the south, shows change either coincident with or somewhat lagged behind the other two records (Fig. 10). This may be a real feature of past atmospheric circulation change, or may be related to the three records' timescales. Regardless, the three records appear to show similar centennial-to-millennial scale variability. It appears that the SWW occupy a more southerly position during periods with negative SOI_{pr} (El Niño), and a more northerly position during periods with positive SOI_{pr} (La Niña). This close correspondence between ENSO and the SWW is consistent with evidence that the central tropical Pacific exerts a strong influence on the high-latitude SH (Schneider and Gies, 2004; Schneider and Steig, 2008; Lamy et al., 2010; Ding et al., 2011, 2012).

4.5 A possible mechanism

A proposed mechanism for SWW latitudinal change on millennial timescales during the last glacial period and termination invokes cold temperatures in the Northern Hemisphere (NH) pushing Earth's thermal equator southward, displacing the SH westerlies poleward (Toggweiler et al., 2006; Denton et al., 2010). While there is increasingly strong evidence to support this bipolar seesaw mechanism on glacial/interglacial timescales (Anderson et al., 2009; Burke and Robinson, 2012; De Deckker et al., 2012), it is less clear how the SWW respond to climate forcing on decadal to centennial timescales. During the LIA, atmospheric cooling, which was greater in the NH (Mann et al., 2009), likely drove the Inter-Tropical Convergence Zone (ITCZ) southward at ~ 1400 C.E., where it remained for ~ 450 yr (Haug et al., 2001; Sachs et al., 2009). Following the mechanism described above, we might expect to see high latitude SH warming and a southward shift of the SWW during this time. However, it appears that

CPD
9, 3125–3174, 2013

the high-latitude SH also cooled, although later than the high-latitude NH (Lowell et al., 2013). From ice core and marine sediment core records, we have good constraints on surface air temperature in West Antarctica (Orsi et al., 2012) and sea surface temperature (SST) on the western side of the Antarctic Peninsula (WAP; Shevenell et al., 2011). Within dating uncertainty, these records show a consistent pattern of cooling during the period ~ 1300–1750 C.E., with perhaps a lead in the surface air temperature (Fig. 8d, e). A record of moss growth from Anvers Island, WAP, indicates that glaciers expanded around 1300 C.E. (Hall et al., 2010), the same time that temperature cooled in the McMurdo Sound region (Bertler et al., 2011). Would this cooling have caused a northward shift of the SWW and contraction of the SH Hadley cell?

Given the evidence described in Sect. 4.4, we suggest that high-latitude SH cooling during the LIA was responsible for a northward shift in the SWW, despite the southerly position of the ITCZ during this time. General circulation model (GCM) experiments have shown that the latitudinal extent of the Hadley cell circulation is sensitive to changes in global surface temperatures, with warmer temperatures causing an expansion of the Hadley cell (Frierson et al., 2007). These changes in the Hadley cell width are likely driven by shifts in the latitude where baroclinic eddies begin to occur; as surface temperatures warm, the transition from baroclinic stability to instability shifts poleward, driving the eddy-driven SH storm track southward (Frierson et al., 2007; Lu et al., 2010). This proposed mechanism implies that the SWW respond to surface temperature changes on decadal to centennial timescales, and need not be driven by NH-induced shifts in the ITCZ. Therefore, it seems possible that the SWW respond to different forcings on different timescales, a condition that may be necessary to reconcile late Holocene and glacial/interglacial SWW reconstructions.

5 Conclusions

We present the first high-resolution microparticle dataset from West Antarctica, spanning the past 2400 yr (430 B.C.E. to 2002 C.E.). We find a particle grain size distribution

CPD
9, 3125–3174, 2013

with a mode diameter in the range of 5–8 µm, comparable to other Antarctic non-EAIS plateau sites. The relative coarseness of particles found in lower-elevation and coastal sites suggests that dust deposited in much of Antarctica has a grain size signature that differs from that of central East Antarctica. Given the relatively coarse size distribution at WAIS Divide, and the similarity in the dust PSD to the theoretical dust emission PSD (Kok, 2011a, b), we infer that there must be an Antarctic dust source supplying central West Antarctica, in addition to potential distal sources such as Australia. Late Holocene dust flux to the WAIS Divide site has remained fairly constant at ~ 3–5 mg m^{-2} yr^{-1}, intermediate between coastal sites in the Weddell Sea region and sites located on the East Antarctic plateau. Observed dust flux differences seem to be driven in part by particle size, which may reflect dust emissions activity near the margins of the Antarctic continent. Further, flux and grain size differences among sites suggest that a substantial amount of dust is transported below ~ 3000 m and does not reach the EAIS plateau.

Supported by terrestrial and marine proxy data from the northern edge to the core of the SWW belt, and based on significant positive correlations with mid-latitude zonal wind speeds, we suggest that changes in the PSD indicate variability in atmospheric circulation intensity in the Amundsen–Bellingshausen Sea region. We infer that the SWW belt shifted poleward during the MCA (~ 950–1350 C.E.) and equatorward during the LIA (~ 1400–1850 C.E.). We suggest that these changes were driven by surface temperature changes and the subsequent expansion/contraction of the SH Hadley cell.

While our record extends only to the past 2400 yr, we believe the relationships shown here are robust. We predict that dust particle data from deeper in the WAIS Divide core will show increased CPP during the early Holocene, indicating a more southerly SWW position when high latitude temperatures were warmer, and decreased CPP during the last glacial period, consistent with a northward shift in the SWW belt and reduced SWW influence in West Antarctica.

CPD
9, 3125–3174, 2013

Acknowledgements. We appreciate helpful discussion with Samuel Albani, Gordon Bromley, Barbara Delmonte, Gang Chen, Jasper Kok, Natalie Mahowald, and Eric Steig. Dianne Dietrich, Jasper Kok, Mark Neary and Huijie Xue helped with software development. We thank Rich Pawlowicz for the m_map plotting package, M. Ma for the wind_rose.m program, Greg Gerbi for help with data filtering, and Urs Ruth and Anna Wegner for assistance setting up and calibrating the Abakus particle counter. David Bromwich and Julien Nicolas provided helpful insights on regional winds and reanalysis data. This paper was improved by helpful comments from Toby Koffman, Stephen Norton, Urs Ruth, and Roberto Udisti. We thank the WAIS Divide Science Coordination Office, Ice Drilling Design and Operations group, the National Ice Core Laboratory, Raytheon Polar Services Company, and the 109th New York Air National Guard. We appreciate the support of the University of Wisconsin–Madison Automatic Weather Station Program for the AWS data set, NSF grant ANT-0944018. This research was funded by NSF grant ANT-0636740, and by the University of Maine Chase Distinguished Research Assistantship, Correll Graduate Student Research Fellowship, and Dissertation Research Fellowship to BGK.

References

Albani, S., Mahowald, N. M., Delmonte, B., Maggi, V., and Winckler, G.: Comparing modeled and observed changes in mineral dust transport and deposition to Antarctica between the Last Glacial Maximum and current climates, Clim. Dynam., 38, 1731–1755, doi:10.1007/s00382-011-1139-5, 2011.

Albani, S., Delmonte, B., Maggi, V., Baroni, C., Petit, J.-R., Stenni, B., Mazzola, C., and Frezzotti, M.: Interpreting last glacial to Holocene dust changes at Talos Dome (East Antarctica): implications for atmospheric variations from regional to hemispheric scales, Clim. Past, 8, 741–750, doi:10.5194/cp-8-741-2012, 2012.

Anderson, R. F., Ali, S., Bradtmiller, L. I., Nielsen, S. H. H., Fleisher, M. Q., Anderson, B. E., and Burckle, L. H.: Wind-driven upwelling in the Southern Ocean and the deglacial rise in atmospheric CO_2, Science, 323, 1443–1448, doi:10.1126/science.1167441, 2009.

Arblaster, J. M. and Meehl, G. A.: Contributions of external forcings to Southern annular mode trends, J. Climate, 19, 2896–2905, 2006.

CPD
9, 3125–3174, 2013

Banta, J. R., McConnell, J. R., Frey, M. M., Bales, R. C., and Taylor, K. C.: Spatial and temporal variability in snow accumulation at the West Antarctic ice sheet divide over recent centuries, J. Geophys. Res., 113, D23102, doi:10.1029/2008JD010235, 2008.

Basile, I., Grousset, F. E., Revel, M., Petit, J. R., Biscaye, P. E., and Barkov, N. I.: Patagonian origin of glacial dust deposited in East Antarctica (Vostok and Dome C) during glacial stages 2, 4 and 6, Earth Planet. Sc. Lett., 146, 573–589, 1997.

Bertler, N. A. N., Mayewski, P., and Carter, L.: Cold conditions in Antarctica during the Little Ice Age – implications for abrupt climate change mechanisms, Earth Planet. Sc. Lett., 308, 41–51, doi:10.1016/j.epsl.2011.05.021, 2011.

Bertler, N. A. N., Mayewski, P., Aristarain, A. J., Barrett, P., Becagli, S., Bernardo, R., Bo, S., Xiao, C., Curran, M., Qin, D., Dixon, D. A., Ferron, F., Fischer, H., Frey, M., Frezzotti, M., Fundel, F., Genthon, C., Gragnani, R., Hamilton, G., Handley, M., Hong, S., Isaksson, E., Kang, J., Ren, J., Kamiyama, K., Kanamori, S., Karkas, E., Karlof, L., Kaspari, S., Kreutz, K., Kurbatov, A., Meyerson, E., Ming, Y., Zhang, M., Motoyama, H., Mulvaney, R., Oerter, H., Osterberg, E., Proposito, M., Pyne, A., Ruth, U., Simoes, J. C., Smith, B., Sneed, S. B., Teinila, K., Traufetter, F., Udisti, R., Virkkula, A., Watanabe, O., Wiliamson, B., Winther, J.-G., Li, Y., Wolff, E., Li, Z., and Zielinski, A.: Snow chemistry across Antarctica, Ann. Glaciol., 41, 167–179, 2005.

Bjorck, S., Rundgren, M., Ljung, K., Unkel, I., and Wallin, A.: Multi-proxy analyses of a peat bog on Isla de los Estados, Easternmost Tierra del Fuego: a unique record of the variable Southern Hemisphere westerlies since the last deglaciation, Quaternary Sci. Rev., 42, 1–14, doi:10.1016/j.quascirev.2012.03.015, 2012.

Bory, A. J.-M., Wolff, E., Mulvaney, R., Jagoutz, E., Wegner, A., Ruth, U., and Elderfield, H.: Multiple sources supply eolian mineral dust to the Atlantic sector of coastal Antarctica: evidence from recent snow layers at the top of Berkner Island ice sheet, Earth Planet. Sc. Lett., 291, 138–148, doi:10.1016/j.epsl.2010.01.006, 2010.

Breton, D. J., Koffman, B. G., Kurbatov, A. V., Kreutz, K. J., and Hamilton, G. S.: Quantifying signal dispersion in a hybrid ice core melting system, Environ. Sci. Technol., 46, 11922–11928, doi:10.1021/es302041k, 2012.

Burke, A. and Robinson, L. F.: The Southern Ocean's role in carbon exchange during the last deglaciation, Science, 335, 557–561, 2012.

Cobb, K. M., Charles, C. D., Cheng, H., and Edwards, R. L.: El Nino/Southern Oscillation and tropical Pacific climate during the last millennium, Nature, 424, 271–276, 2003.

CPD
9, 3125–3174, 2013

De Deckker, P., Moros, M., Perner, K., and Jansen, E.: Influence of the tropics and southern westerlies on glacial interhemispheric asymmetry, Nat. Geosci., 5, 266–269, doi:10.1038/NGEO1431, 2012.

Dee, D. P., Uppala, S. M., Simmons, A. J., Berrisford, P., Poli, P., Kobayashi, S., Andrae, U., Balmaseda, M. A., Balsamo, G., Bauer, P., Bechtold, P., Beljaars, A. C. M., van de Berg, L., Bidlot, J., Bormann, N., Delsol, C., Dragani, R., Fuentes, M., Geer, A. J., Haimberger, L., Healy, S. B., Hersbach, H., Holm, E. V., Isaksen, L., Kallberg, P., Kohler, M., Matricardi, M., McNally, A. P., Monge-Sanz, B. M., Morcrette, J.-J., Park, B.-K., Peubey, C., de Rosnay, P., Tavolato, C., Thepaut, J.-N., and Vitart, F.: The ERA-Interim reanalysis: configuration and performance of the data assimilation system, Q. J. Roy. Meteor. Soc., 137, 553–597, 2011.

Delmonte, B., Petit, J.-R., and Maggi, V.: Glacial to Holocene implications of the new 27 000-year dust record from the EPICA Dome C (East Antarctica) ice core, Clim. Dynam., 18, 647–660, doi:10.1007/s00382-001-0193-9, 2002.

Delmonte, B., Basile-Doelsch, I., Petit, J. R., Maggi, V., Revel-Rolland, M., Michard, A., Jagoutz, E., and Grousset, F.: Comparing the Epica and Vostok dust records during the last 220 000 years: stratigraphical correlation and provenance in glacial periods, Earth-Sci. Rev., 66, 63–87, 2004.

Delmonte, B., Petit, J. R., Krinner, G., Maggi, V., Jouzel, J., and Udisti, R.: Ice core evidence for secular variability and 200-year dipolar oscillations in atmospheric circulation over East Antarctica during the Holocene, Clim. Dynam., 24, 641–654, 2005.

Delmonte, B., Andersson, P. S., Hansson, M., Schoberg, H., Petit, J. R., Basile-Doelsch, I., and Maggi, V.: Aeolian dust in East Antarctica (EPICA-Dome C and Vostok): provenance during glacial ages of the last 800 kyr, Geophys. Res. Lett., 35, L07703, doi:10.1029/2008GL033382, 2008.

Delmonte, B., Andersson, P. S., Schoberg, H., Hansson, M., Petit, J. R., Delmas, R., Gaiero, D. M., Maggi, V., and Frezzotti, M.: Geographic provenance of aeolian dust in East Antarctica during Pleistocene glaciations: preliminary results from Talos Dome and comparison with East Antarctic and new Andean ice core data, Quaternary Sci. Rev., 29, 256–264, doi:10.1016/j.quascirev.2009.05.010, 2010.

Denton, G. H., Anderson, R. F., Toggweiler, J. R., Edwards, R. L., Schaefer, J. M., and Putnam, A. E.: The last glacial termination, Science, 328, 1652–1656, 2010.

Ding, Q., Steig, E., Battisti, D. S., and Kuttel, M.: Winter warming in West Antarctica caused by central tropical Pacific warming, Nat. Geosci., 4, 398–403, doi:10.1038/NGEO1129, 2011.

CPD
9, 3125–3174, 2013

Ding, Q., Steig, E. J., Battisti, D. S., and Wallace, J. M.: Influence of the tropics on the southern annular mode, J. Climate, 25, 6330–6348, doi:10.1175/JCLI-D-11-00523.1, 2012.
Dixon, D. A., Mayewski, P. A., Goodwin, I. D., Marshall, G. J., Freeman, R., Maasch, K. A., and Sneed, S.: An ice core proxy for northerly air mass incursions (NAMI) into West Antarctica, Int. J. Climatol., 2, 1455-1465, doi:10.1002/joc.2371, 2012.
Edwards, R., Sedwick, P., Morgan, V., and Boutron, C.: Iron in ice cores from Law Dome: a record of atmospheric iron deposition for maritime East Antarctica during the Holocene and Last Glacial Maximum, Geochem. Geophys. Geosyst., 7, Q12Q01, doi:10.1029/2006/GC001307, 2006.
Fischer, H., Siggaard-Andersen, M.-L., Ruth, U., Rothlisberger, R., and Wolff, E.: Glacial/interglacial changes in mineral dust and sea-salt records in polar ice cores: sources, transport, and deposition, Rev. Geophys., 45, 1, doi:10.1029/2005RG000192, 2007.
Fletcher, M.-S. and Moreno, P. I.: Zonally symmetric changes in the strength and position of the Southern westerlies drove atmospheric CO_2 variations over the past 14 k.y., Geology, 39, 419–422, doi:10.1130/G31807.1, 2011.
Fletcher, M.-S. and Moreno, P. I.: Have the southern westerlies changed in a zonally symmetric manner over the last 14 000 years? A hemisphere-wide take on a controversial problem, Quaternary Int., 253, 32–46, doi:10.1016/j.quaint.2011.04.042, 2012a.
Fletcher, M.-S., and Moreno, P. I.: Vegetation, climate and fire regime changes in the Andean region of southern Chile (38°S) covaried with centennial-scale climate anomalies in the tropical Pacific over the last 1500 years, Quaternary Sci. Rev., 46, 46–56, doi:10.1016/j.quascirev.2012.04.016, 2012b.
Frierson, D. M. W., Lu, J., and Chen, G.: Width of the Hadley cell in simple and comprehensive general circulation models, Geophys. Res. Lett., 34, L18804, doi:10.1029/2007GL031115, 2007.
Gaspari, V., Barbante, C., Cozzi, G., Cescon, P., Boutron, C. F., Gabrielli, P., Capodaglio, G., Ferrari, C., Petit, J. R., and Delmonte, B.: Atmospheric iron fluxes over the last deglaciation: climatic implications, Geophys. Res. Lett., 33, L03704, doi:10.1029/2005GL024352, 2006.
Goodwin, I. D., van Ommen, T. D., Curran, M. A. J., and Mayewski, P. A.: Mid latitude winter climate variability in the South Indian and southwest Pacific regions since 1300 AD, Clim. Dynam., 22, 783–794, doi:10.1007/s00382-004-0403-3, 2004.
Hall, B. L., Koffman, T., and Denton, G. H.: Reduced ice extent on the western Antarctic Peninsula at 700–970 cal. yr B.P., Geology, 38, 635–638, doi:10.1130/G30932.1, 2010.

CPD
9, 3125–3174, 2013

Haug, G. H., Hughen, K. A., Sigman, D. M., Peterson, L. C., and Rohl, U.: Southward migration of the intertropical convergence zone through the Holocene, Science, 293, 1304–1308, 2001.

Knudson, K. P., Hendy, I. L., and Neil, H. L.: Re-examining Southern Hemisphere westerly wind behavior: insights from a late Holocene precipitation reconstruction using New Zealand fjord sediments, Quaternary Sci. Rev., 30, 3124–3138, doi:10.1016/j.quascirev.2011.07.017, 2011.

Kok, J. F.: A scaling theory for the size distribution of emitted dust aerosols suggests climate models underestimate the size of the global dust cycle, P. Natl. Acad. Sci. USA, 108, 1016–1021, doi:10.1073/pnas.1014798108, 2011a.

Kok, J. F.: Does the size distribution of mineral dust aerosols depend on the wind speed at emission?, Atmos. Chem. Phys., 11, 10149–10156, doi:10.5194/acp-11-10149-2011, 2011b.

Kreutz, K. J., Mayewski, P. A., Meeker, L. D., Twickler, M. S., Whitlow, S. I., and Pittalwala, I. I.: Bipolar changes in atmospheric circulation during the Little Ice Age, Science, 277, 1294–1296, 1997.

Kreutz, K. J., Mayewski, P. A., Meeker, L. D., Twickler, M. S., and Whitlow, S. I.: The effect of spatial and temporal accumulation rate variability in West Antarctica on soluble ion deposition, Geophys. Res. Lett., 27, 2517–2520, 2000a.

Kreutz, K. J., Mayewski, P. A., Pittalwala, I. I., Meeker, L. D., Twickler, M. S., and Whitlow, S. I.: Sea level pressure variability in the Amundsen Sea region inferred from a West Antarctic glaciochemical record, J. Geophys. Res., 105, 4047–4059, 2000b.

Krinner, G., Petit, J.-R., and Delmonte, B.: Altitude of atmospheric trace transport toward Antarctica in present and glacial climate, Quaternary Sci. Rev., 29, 274–284, doi:10.1016/j.quascirev.2009.06.020, 2010.

Lambert, F., Delmonte, B., Petit, J.-R., Bigler, M., Kaufmann, P., Hutterli, M. A., Stocker, T., and Ruth, U.: Dust-climate couplings over the past 800 000 years from the EPICA Dome C ice core, Nature, 452, 616–619, doi:10.1038/nature06763, 2008.

Lambert, F., Bigler, M., Steffensen, J. P., Hutterli, M., and Fischer, H.: Centennial mineral dust variability in high-resolution ice core data from Dome C, Antarctica, Clim. Past, 8, 609–623, doi:10.5194/cp-8-609-2012, 2012.

Lamy, F., Hebbeln, D., Rohl, U., and Wefer, G.: Holocene rainfall variability in southern Chile: a marine record of latitudinal shifts of the southern westerlies, Earth Planet. Sc. Lett., 185, 369–382, 2001.

CPD
9, 3125–3174, 2013

Lamy, F., Kilian, R., Arz, H. W., Francois, J.-P., Kaiser, J., Prange, M., and Steinke, T.: Holocene changes in the position and intensity of the southern westerly wind belt, Nat. Geosci., 3, 695–699, 2010.

Lazzara, M. A., Weidner, G. A., Keller, L. M., Thom, J. E., and Cassano, J. J.: Antarctic automatic weather station program: 30 years of polar observations, B. Am. Meteorol. Soc., 93(, 1519–1537, 2012.

Lee, S. and Feldstein, S. B.: Detecting ozone- and greenhouse gas-driven wind trends with observational data, Science, 339, 563–567, 2013.

Legrand, M. and Mayewski, P.: Glaciochemistry of polar ice cores: a review, Rev. Geophys., 35, 219–243, 1997.

Lenton, A., Codron, F., Bopp, L., Metzl, N., Cadule, P., Tagliabue, A., and Le Sommer, J.: Stratospheric ozone depletion reduces ocean carbon uptake and enhances ocean acidification, Geophys. Res. Lett., 36, L12606, doi:10.1029/2009GL038227, 2009.

Lenton, A., Metzl, N., Takahashi, T., Kuchinke, M., Matear, R. J., Roy, T., Sutherland, S. C., Sweeney, C., and Tilbrook, B.: The observed evolution of oceanic pCO_2 and its drivers over the last two decades, Global Biogeochem. Cy., 26, GB2021, doi:10.1029/2011GB004095, 2012.

Li, F., Ginoux, P., and Ramaswamy, V.: Distribution, transport, and depositon of mineral dust in the Southern Ocean and Antarctica: contribution of major sources, J. Geophys. Res., 113, D10207, doi:10.1029/2007JD009190, 2008.

Lowell, T. V., Hall, B. L., Kelly, M. A., Bennike, O., Lusas, A. R., Honsaker, W., Smith, C. A., Levy, L. B., Travis, S., and Denton, G. H.: Late Holocene expansion of Istorvet ice cap, Liverpool Land, east Greenland, Quaternary Sci. Rev., 63, 128–140, doi:10.1016/j.quascirev.2012.11.012, 2013.

Lu, J., Chen, G., and Frierson, D. M. W.: The position of the midlatitude storm track and eddy-driven westerlies in Aquaplanet AGCMs, J. Atmos. Sci., 67, 3984–4000, doi:10.1175/2010JAS3477.1, 2010.

Lubin, D., Wittenmyer, R. A., Bromwich, D. H., and Marshall, G. J.: Antarctic Peninsula mesoscale cyclone variability and climatic impacts influenced by the SAM, Geophys. Res. Lett., 35, L02808, doi:10.1029/2007GL032170, 2008.

Maasch, K. A., Mayewski, P. A., Rohling, E. J., Stager, J. C., Karlen, W., Meeker, L. D., and Meyerson, E. A.: A 2000-year context for modern climate change, Geogr. Ann., 87, 7–15, 2005.

CPD
9, 3125–3174, 2013

Mann, M. E., Zhang, Z., Rutherford, S., Bradley, R. S., Hughes, M. K., Shindell, D. T., Ammann, C., Faluvegi, G., and Ni, F.: Global signatures and dynamical origins of the Little Ice Age and medieval climate anomaly, Science, 326, 1256–1260, doi:10.1126/science.1177303, 2009.

Marino, F., Castellano, E., Ceccato, D., De Deckker, P., Delmonte, B., Ghermandi, G., Maggi, V., Petit, J. R., Revel-Rolland, M., and Udisti, R.: Defining the geochemical composition of the EPICA Dome C ice core dust during the last glacial-interglacial cycle, Geochem. Geophys. Geosys., 9, Q10018, doi:10.1029/2008GC002023, 2008.

Marino, F., Castellano, E., Nava, S., Chiari, M., Ruth, U., Wegner, A., Lucarelli, F., Udisti, R., Delmonte, B., and Maggi, V.: Coherent composition of glacial dust on opposite sides of the East Antarctic Plateau inferred from the deep EPICA ice cores, Geophys. Res. Lett., 36, L23703, doi:10.1029/2009GL040732, 2009.

Martinez-Garcia, A., Rosell-Mele, A., Jaccard, S. L., Geibert, W., Sigman, D. M., and Haug, G. H.: Southern Ocean dust-climate coupling over the past four million years, Nature, 476, 312–315, 2011.

Mayewski, P. A., Meeker, L. D., Whitlow, S. I., Twickler, M. S., Morrison, M. C., Grootes, P. M., Bond, G. C., Alley, R. B., Meese, D. A., Gow, A. J.,Taylor, K. C. , Ram, M., and Wumkes, M.: Changes in atmospheric circulation and ocean ice cover over the North Atlantic during the last 41 000 years, Science, 263, 1747–1751, 1994.

Mayewski, P. A., Meredith, M., Summerhayes, C., Turner, J., Aoki, S., Barrett, P., Bertler, N. A. N., Bracegirdle, T., Bromwich, D., Campbell, H., Casassa, G., Garabato, A. N., Lyons, W. B., Maasch, K. A., Worby, A., and Xiao, C.: State of the Antarctic and Southern Ocean Climate System, Rev. Geophys., 47, RG1003, doi:10.1029/2007RG000231, 2009.

Mayewski, P., Maasch, K. A., Dixon, D. A., Sneed, S. B., Oglesby, R., Korotkikh, E., Potocki, M., Grigholm, B., Kreutz, K., Kurbatov, A., Spaulding, N., Stager, J. C., Taylor, K. C., Steig, E., White, J., Bertler, N. A. N., Goodwin, I., Simoes, J. C., Jana, R., Kraus, S., and Fastook, J.: West Antarctica's sensitivity to natural and human-forced climate change over the Holocene, J. Quaternary Sci., 28, 40–48, 2013.

McConnell, J. R., Aristarain, A. J., Banta, J. R., Edwards, P. R., and Simoes, J. C.: 20th-Century doubling in dust archived in an Antarctic Peninsula ice core parallels climate change and desertification in South America, P. Natl. Acad. Sci. USA, 104, 5743–5748, 2007.

McGee, D., Broecker, W. S., and Winckler, G.: Gustiness: The driver of glacial dustiness?, Quaternary Sci. Rev., 29, 2340–2350, 2010.

CPD
9, 3125–3174, 2013

Moreno, P. I., Francois, J. P., Villa-Martinez, R. P., and Moy, C. M.: Millennial-scale variability in Southern Hemisphere westerly wind activity over the last 5000 years in SW Patagonia, Quaternary Sci. Rev., 28, 25–38, doi:10.1016/j.quascirev.2008.10.009, 2009.
Moreno, P. I., Francois, J. P., Moy, C. M., and Villa-Martinez, R.: Covariability of the Southern Westerlies and atmospheric CO_2 during the Holocene, Geology, 38, 727–730, 2010.
Mosley-Thompson, E. and Thompson, L. G.: Nine centuries of microparticle deposition at the South Pole, Quaternary Res., 17, 1–13, 1982.
Mosley-Thompson, E. and Thompson, L. G.: Little Ice Age (Neoglacial) paleoenvironmental conditions at Siple Station, Antarctica, Ann. Glaciol., 14, 199–204, 1990.
Moy, C. M., Seltzer, G. O., Rodbell, D. T., and Anderson, D. M.: Variability of El Nino/Southern oscillation activity at millennial timescales during the Holocene epoch, Nature, 420, 162–165, 2002.
Moy, C. M., Dunbar, R. B., Moreno, P. I., Francois, J.-P., Villa-Martinez, R., Mucciarone, D. M., Guilderson, T. P., and Garreaud, R. D.: Isotopic evidence for hydrologic change related to the westerlies in SW Patagonia, Chile, during the last millennium, Quaternary Sci. Rev., 27, 1335–1349, doi:10.1016/j.quascirev.2008.03.006, 2008.
Nicolas, J. P. and Bromwich, D. H.: Climate of West Antarctica and influence of marine air intrusions, J. Climate, 24, 49–67, doi:10.1075/2010JCLI3522.1, 2011.
O'Brien, S. R., Mayewski, P. A., Meeker, L. D., Meese, D. A., Twickler, M. S., and Whitlow, S. I.: Complexity of Holocene climate as reconstructed from a Greenland ice core, Science, 270, 1962–1963, 1995.
Orsi, A. J., Cornuelle, B. D., and Severinghaus, J. P.: Little Ice Age cold interval in West Antarctica: evidence from borehole temperature at the West Antarctic Ice Sheet (WAIS) divide, Geophys. Res. Lett., 39, L09710, doi:10.1029/2012GL051260, 2012.
Petit, J. R., Jouzel, J., Raynaud, D., Barkov, N. I., Barnola, J. M., Basile, I., Bender, M., Chappellaz, J., Davis, M., Delaygue, G., Delmotte, M., Kotlyakov, V. M., Legrand, M., Lipenkov, V. Y., Lorius, C., Pepin, L., Ritz, C., Saltzman, E., and Stievenard, M.: Climate and atmospheric history of the past 420 000 years from the Vostok ice core, Antarctica, Nature, 399, 429–436, 1999.
Rankin, A. M. and Wolff, E.: Frost flowers: implications for tropospheric chemistry and ice core interpretation, J. Geophys. Res., 107, 4683, doi:10.1029/2002JD002492, 2002.
Rankin, A. M., Auld, V., and Wolff, E. W.: Frost flowers as a source of fractionated sea salt aerosol in the polar regions, Geophys. Res. Lett., 27, 3469–3472, 2000.

CPD
9, 3125–3174, 2013

Renssen, H., Goosse, H., Fichefet, T., Masson-Delmotte, V., and Koc, N.: Holocene climate evolution in the high-latitude Southern Hemisphere simulated by a coupled atmosphere-sea ice-ocean-vegetation model, Holocene, 15, 951–964, doi:10.1191/0959683605hl869ra, 2005.

Russell, J. L., Dixon, K. W., Gnanadesikan, A., Stouffer, R. J., and Toggweiler, J. R.: The Southern Hemisphere westerlies in a warming world: propping open the door to the deep ocean, J. Climate, 19, 6382–6390, 2006.

Ruth, U., Wagenbach, D., Steffensen, J. P., and Bigler, M.: Continuous record of microparticle concentration and size distribution in the central Greenland NGRIP ice core during the last glacial period, J. Geophys. Res., 108, 4098, doi:10.1029/2002JD002376, 2003.

Ruth, U., Wagenbach, D., Mulvaney, R., Oerter, H., Graf, W., Pulz, H., and Littot, G.: Comprehensive 1000 year climatic history from an intermediate-depth ice core from the south dome of Berkner Island, Antarctica: methods, dating and first results, Ann. Glaciol., 39, 146–154, 2004.

Ruth, U., Barbante, C., Bigler, M., Delmonte, B., Fischer, H., Gabrielli, P., Gaspari, V., Kaufmann, P., Lambert, F., Maggi, V., Marino, F., Petit, J.-R., Udisti, R., Wagenbach, D., Wegner, A., and Wolff, E. W.: Proxies and measurement techniques in antarctic ice cores, Environ. Sci. Technol., 42, 5675–5681, doi:10.1021/es703078z, 2008.

Sachs, J. P., Sachse, D., Smittenberg, R. H., Zhang, Z., Battisti, D. S., and Golubic, S.: Southward movement of the Pacific intertropical convergence zone AD 1400–1850, Nat. Geosci., 2, 519–525, doi:10.1038/NGEO554, 2009.

Saunders, K. M., Kamenik, C., Hodgson, D. A., Hunziker, S., Siffert, L., Fischer, D., Fujak, M., Gibson, J. A. E., and Grosjean, M.: Late Holocene changes in precipitation in northwest Tasmania and their potential links to shifts in the Southern Hemisphere westerly winds, Global Planet. Change, 92–93, 82–91, doi:10.1016/j.glopacha.2012.04.005, 2012.

Schneider, C. and Gies, D.: Effects of El Nino-Southern Oscillation on southernmost South America precipitation at 53° S revealed from NCEP-NCAR reanalyses and weather station data, Int. J. Climatol., 24, 1057–1076, doi:10.1002/joc.1057, 2004.

Schneider, D. P. and Steig, E. J.: Ice cores record significant 1940s Antarctic warmth related to tropical climate variability, P. Natl. Acad. Sci. USA, 105, 12154–12158, 2008.

Shevenell, A. E., Ingalls, A. E., Domack, E. W., and Kelly, C.: Holocene Southern Ocean surface temperature variability west of the Antarctic Peninsula, Nature, 470, 250–254, doi:10.1038/nature09751, 2011.

CPD
9, 3125–3174, 2013

Stager, J. C., Mayewski, P. A., White, J., Chase, B. M., Neumann, F. H., Meadows, M. E., King, C. D., and Dixon, D. A.: Precipitation variability in the winter rainfall zone of South Africa during the last 1400 yr linked to the austral westerlies, Clim. Past, 8, 877–887, doi:10.5194/cp-8-877-2012, 2012.

Steffensen, J. P.: The size distribution of microparticles from selected segments of the Greenland Ice Core Project ice core representing different climatic periods, J. Geophys. Res., 102, 26755–26763, 1997.

Stuiver, M., Grootes, P. M., and Braziunas, T. F.: The GISP2 $\delta^{18}O$ climate record of the past 16,500 years and the role of the Sun, oceans, and volcanoes, Quaternary Res., 44, 341–354, 1995.

Sugden, D. E., McCulloch, R. D., Bory, A. J.-M., and Hein, A. S.: Influence of Patagonian glaciers on Antarctic dust deposition during the last glacial period, Nat. Geosci., 2, 281–285, doi:10.1038/NGEO474, 2009.

Takahashi, T., Sutherland, S. C., Sweeney, C., Poisson, A., Metzl, N., Tilbrook, B., Bates, N., Wanninkhof, R., Feely, R. A., Sabine, C., Olafsson, J., and Nojiri, Y.: Global sea-air CO_2 flux based on climatological surface ocean pCO_2, and seasonal biological and temperature effects, Deep-Sea Res. Pt. II, 49, 1601–1622, 2002.

Thompson, D. W. J. and Solomon, S.: Interpretation of recent Southern Hemisphere climate change, Science, 296, 895–899, 2002.

Thompson, D. W. J., Solomon, S., Kushner, P. J., England, M. H., Grise, K. M., and Karoly, D. J.: Signatures of the Antarctic ozone hole in Southern Hemisphere surface climate change, Nat. Geosci., 4, 741–749, doi:10.1038/NGEO1296, 2011.

Thompson, L. G.: Variations in microparticle concentration, size distribution and elemental composition found in Camp Century, Greenland, and Byrd station, Antarctica deep ice cores, Isotopes and Impurities in Snow and Ice Symposium, in: Proceedings of the Grenoble Symposium, 351–364, August, 1977.

Toggweiler, J. R., Russell, J. L., and Carson, S. R.: Midlatitude westerlies, atmospheric CO_2, and climate change during the ice ages, Paleoceanography, 21, PA2005, doi:10.1029/2005PA001154, 2006.

Turner, D. R. and Hunter, K. A. (Eds.): The Biogeochemistry of Iron in Seawater, John T. Wiley & Sons, Ltd., Chichester, England, 2001.

CPD
9, 3125–3174, 2013

Turner, J., Bindschadler, R. A., Convey, P., Di Prisco, G., Fahrbach, E., Gutt, J., Hodgson, D. A., Mayewski, P. A., and Summerhayes, C. P. (Eds.): Antarctic Climate Change and the Environment, Scientific Committee on Antarctic Research, Cambridge, 2009.

Vance, T., van Ommen, T. D., Curran, M. A. J., and Plummer, C. T.: A millennial proxy record of ENSO and eastern Australian rainfall from the Law Dome ice core, East Antarctica, J. Climate, 26, 710–725, doi:10.1175/JCLI-D-12-00003.1, 2013.

Varma, V., Prange, M., Merkel, U., Kleinen, T., Lohmann, G., Pfeiffer, M., Renssen, H., Wagner, A., Wagner, S., and Schulz, M.: Holocene evolution of the Southern Hemisphere westerly winds in transient simulations with global climate models, Clim. Past, 8, 391–402, doi:10.5194/cp-8-391-2012, 2012.

Wagenbach, D., Ducroz, F., Mulvaney, R., Keck, L., Minikin, A., Legrand, M., Hall, J. S., and Wolff, E.: Sea-salt aerosol in coastal Antarctic regions, J. Geophys. Res., 103, 10961–10974, 1998.

WAIS Divide Project Members, Fudge, T. J., Steig, E. J., Markle, B. R., Taylor, K. C., McConnell, J. R., Brook, E. J., Sowers, T., White, J. W. C., Schoenemann, S. W., Alley, R. B., Cheng, H., Clow, G. D., Cole-Dai, J., Conway, H., Cuffey, K. M., Edwards, J. S., Edwards, R. L., Edwards, R., Fegyveresi, J. M., Ferris, D. G., Fitzpatrick, J. J., Johnson, J., Hargreaves, G., Lee, J. E., Maselli O. J., Mason, W., McGwire, K. C., Mitchell, L. E., Mortensen, N., Neff, P., Orsi, A. J., Schauer, A. J., Severinghaus, J. P., Sigl, M., Spencer, M. K., Vaughn, B. H., Voigt, D. E., Waddington, E., Wang, X., and Wong, G. J.: Deglacial warming in West Antarctica driven by both local orbital and Northern Hemisphere forcing, Nature, in review, 2013.

Waugh, D. W., Primeau, F., DeVries, T., and Holzer, M.: Recent changes in the ventilation of the Southern Oceans, Science, 339, 568–570, doi:10.1126/science.1225411, 2013.

Wegner, A., Gabrielli, P., Wilhelms-Dick, D., Ruth, U., Kriews, M., De Deckker, P., Barbante, C., Cozzi, G., Delmonte, B., and Fischer, H.: Change in dust variability in the Atlantic sector of Antarctica at the end of the last deglaciation, Clim. Past, 8, 135–147, doi:10.5194/cp-8-135-2012, 2012.

Wolff, E., Rankin, A. M., and Rothlisberger, R.: An ice core indicator of Antarctic sea ice production?, Geophys. Res. Lett., 30, 2158, doi:10.1029/2003GL018454, 2003.

Wolff, E. W., Fischer, H., Fundel, F., Ruth, U., Twarloh, B., Littot, G. C., Mulvaney, R., Rothlisberger, R., de Angelis, M., Boutron, C., Hansson, M., Jonsell, U., Hutterli, M. A., Lambert, F., Kaufmann, P., Stauffer, B., Stocker, T. F., Steffensen, J. P., Bigler, M., Siggaard-Andersen, M.-L., Udisti, R., Becagli, S., Castellano, E., Severi, M., Wagenbach, D., Barbante, C., Gabrielli,

CPD
9, 3125–3174, 2013

P., and Gaspari, V.: Southern Ocean sea-ice extent, productivity and iron flux over the past eight glacial cycles, Nature, 440, 491–496, doi:10.1038/nature04614, 2006.
Wu, G., Yao, T., Xu, B., Tian, L., Zhang, C., and Zhang, X.: Volume-size distribution of microparticles in ice cores from the Tibetan Plateau, J. Glaciol., 55, 859–868, 2009.
Yan, H., Sun, L., Wang, Y., Huang, W., Qiu, S., and Yang, C.: A record of the Southern Oscillation Index for the past 2,000 years from precipitation proxies, Nat. Geosci., 4, 611–614, doi:10.1038/NGEO1231, 2011.
Yan, Y., Mayewski, P. A., Kang, S., and Meyerson, E.: An ice core proxy for Antarctic circumpolar zonal wind intensity, Ann. Glaciol., 41, 121–130, 2005.

CPD
9, 3125–3174, 2013

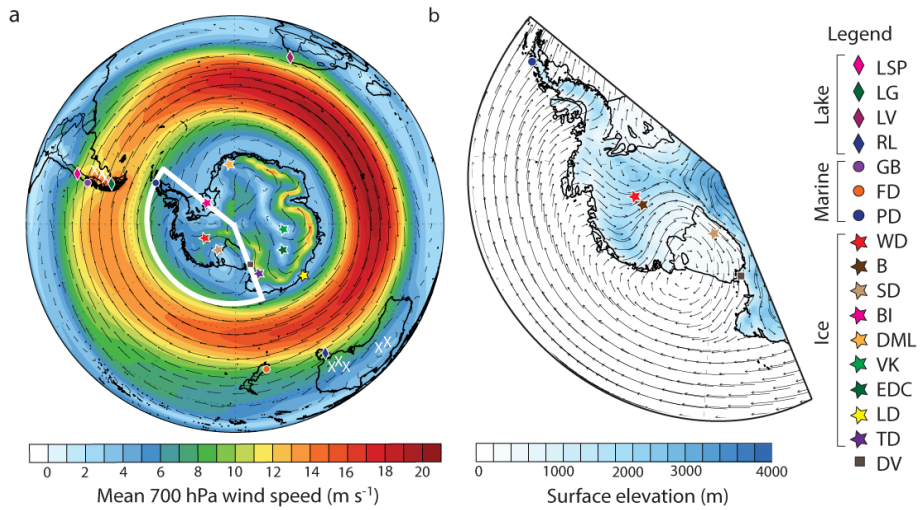

Fig. 1. (a) Map of the Southern Hemisphere showing mean (1979–2010) annual wind speed (colors) and direction (vectors) at 700 hPa from ERA-Interim reanalysis data, major SH dust sources (white Xs) and locations of sites discussed in the text, as indicated (Lake cores: LSP: Laguna San Pedro; LG: Lago Guanaco; LV: Lake Verlorenvlei; RL: Rebecca Lagoon. Marine cores: GB: GeoB 3313-1; FD: Fiordland; PD: Palmer Deep. Ice cores: WD: WAIS Divide; B: Byrd; SD: Siple Dome; BI: Berkner Island; DML: EPICA Dronning Maud Land; VK: Vostok; EDC: EPICA Dome C; LD: Law Dome; TD: Talos Dome. DV: Dry Valleys). **(b)** Map of the WAIS region showing elevation (blue shading), annual average 700 hPa wind vectors from ERA-Interim reanalysis data, and site locations, as indicated.

CPD
9, 3125–3174, 2013

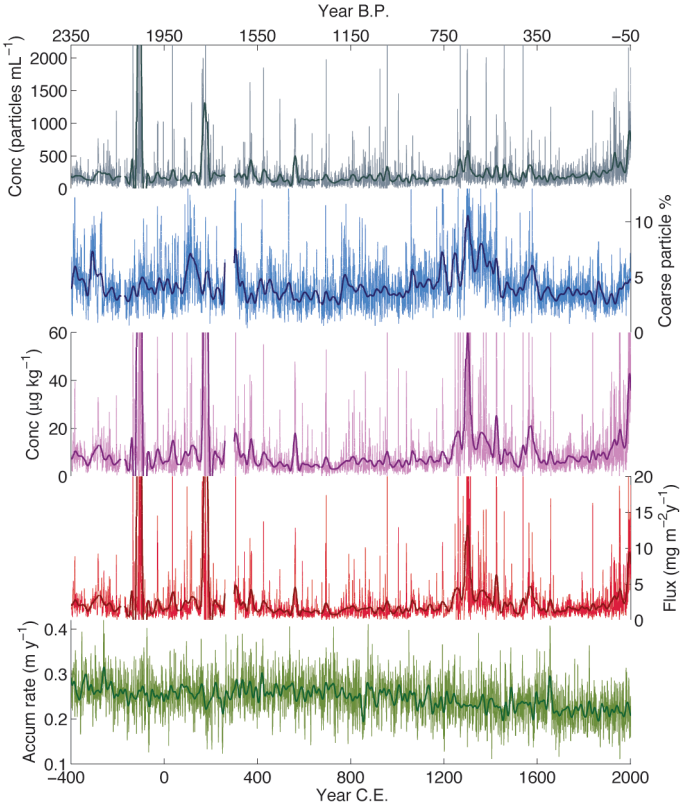

Fig. 2. Dust time series plots: **(a)** dust number concentration; **(b)** coarse particle percentage (CPP, defined as number of particles mL^{-1} [4.5–15]/[1–15] µm diameter ×100); **(c)** dust mass concentration; **(d)** dust flux; and **(e)** accumulation rate in m water equivalent (from WAIS Divide Project Members, 2013). Thin lines show one-year filtered data and thick lines show 21 yr filtered data, except for **(e)**, for which the raw data are annual (thin line); in this case the thick line shows the 21 yr filtered record.

CPD
9, 3125–3174, 2013

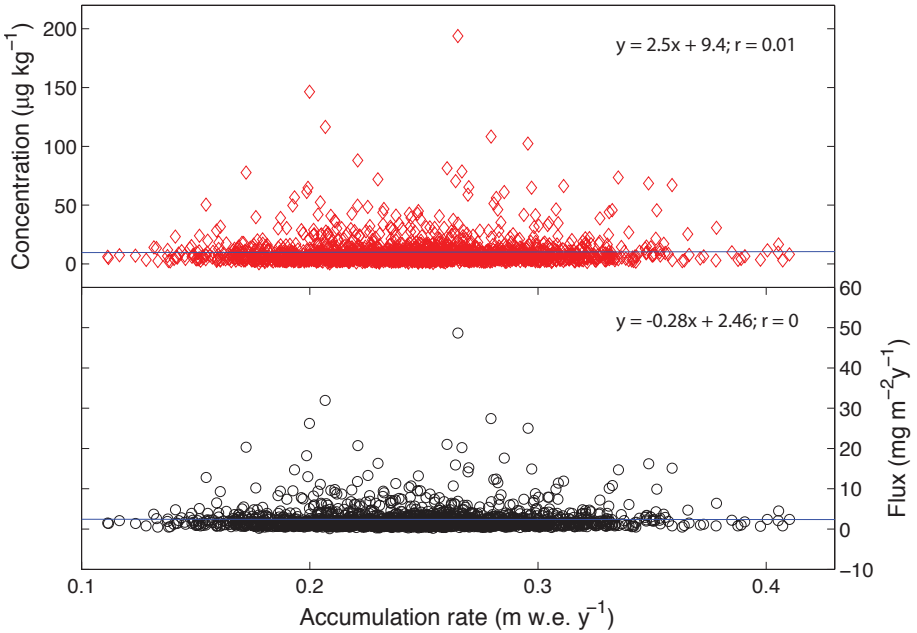

Fig. 3. Dust concentration and flux plotted vs. accumulation rate; linear regressions are given.

CPD
9, 3125–3174, 2013

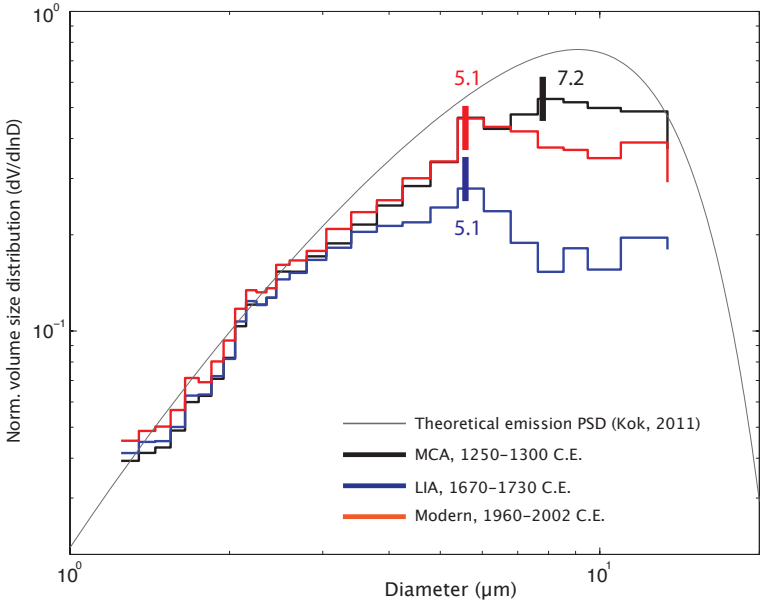

Fig. 4. Normalized volume size distribution, dV/d$\ln D$, for three representative time periods along with theoretical dust emission PSD formulated by Kok (2011b). Vertical colored bars indicate the mode (most commonly occurring value) of each distribution. It is evident that while the modern mode is the same as that during the LIA, there is a greater contribution of coarse particles compared to the LIA period.

CPD
9, 3125–3174, 2013




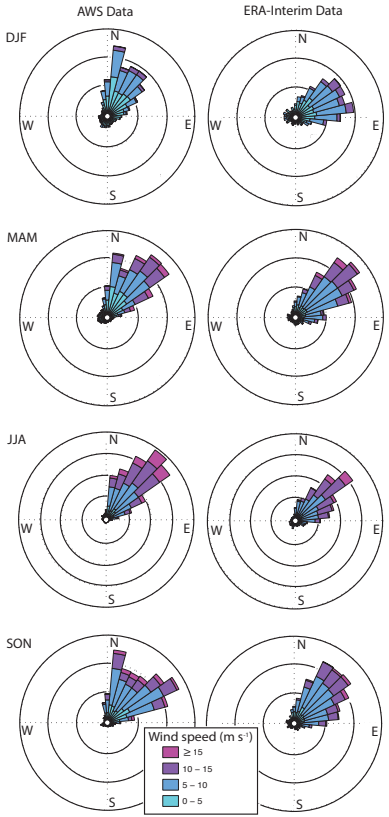

Fig. 5. Automatic weather station (left) and ERA-Interim (right) surface wind speed and direction data by season from the WAIS Divide site. Wind rose plots show the frequency with which winds came from a given direction. Each dotted circle represents 5 % of observations. True cardinal directions are indicated.

CPD
9, 3125–3174, 2013

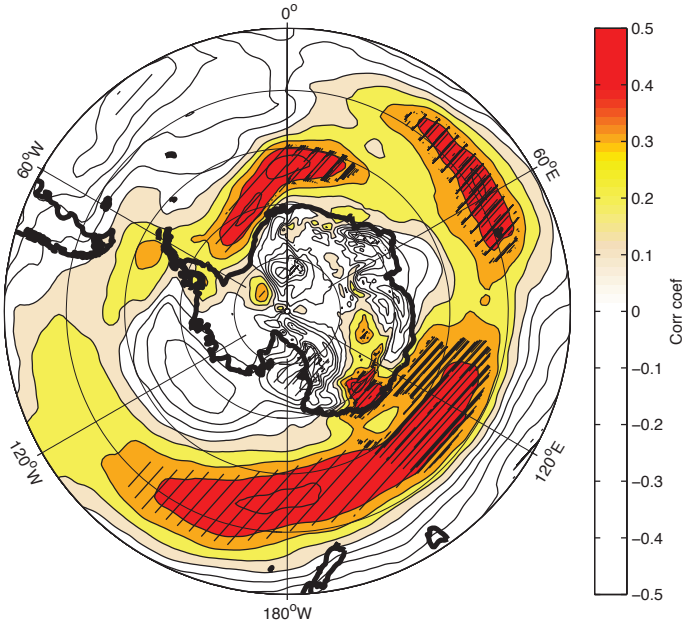

Fig. 6. Spatial correlation map showing Pearson's linear correlation coefficient (colors) and regions of 90 % significance (hatching) for correlation between WAIS Divide CPP and annual mean 700 hPa zonal wind speed for the interval 1979–2002. For clarity, we have colored only regions of positive correlation.

CPD
9, 3125–3174, 2013

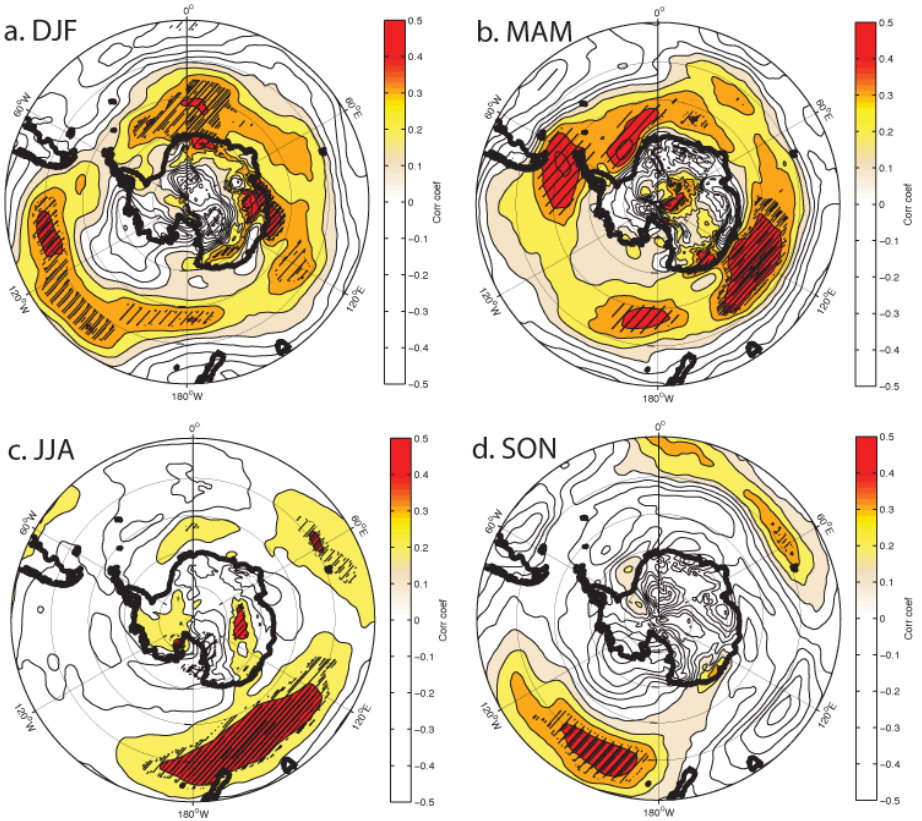

Fig. 7. Spatial correlation maps showing Pearson's linear correlation coefficient (colors) and regions of 90 % significance (hatching) for correlations between WAIS Divide CPP and seasonal mean 700 hPa zonal wind speed for **(a)** summer (DJF), **(b)** fall (MAM), **(c)** winter (JJA), and **(d)** spring (SON) seasons for the interval 1979–2002. For clarity, we have colored only regions of positive correlation.

CPD
9, 3125–3174, 2013

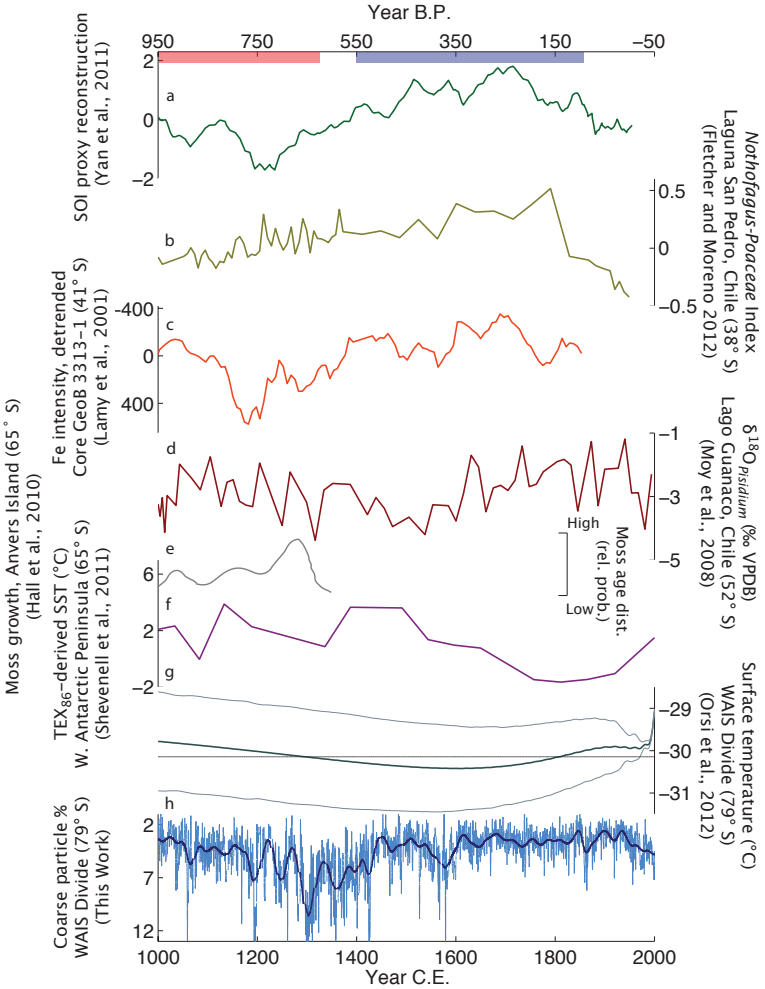

Fig. 8. Caption on next page.

CPD
9, 3125–3174, 2013

Fig. 8. Paleoclimate reconstructions from the eastern Pacific region: **(a)** Southern Oscillation Index (SOI) precipitation-based reconstruction; negative values indicate a more El Niño-like state (Yan et al., 2011). **(b)** *Nothofagus-Poaceae* Index (NPI) from Laguna San Pedro, Chile; increased (positive) NPI indicates *Nothofagus* (southern beech) expansion due to SWW-driven precipitation in the region (Fletcher and Moreno, 2012b). **(c)** Detrended iron intensity record from marine sediment core GeoB 3313–1 on an inverted axis; low values indicate more humid conditions (Lamy et al., 2001). **(d)** Lago Guanaco, Chile δ^{18}O of *Pisidium* bivalve shells (Moy et al., 2008). Less-negative δ^{18}O values are associated with increased evaporation, due to a variable combination of surface air temperature and wind speed (see text). **(e)** Relative probability distribution of in situ moss growing on Anvers Island, Antarctica (Hall et al., 2010). **(f)** Reconstructed SST from Palmer Deep, Antarctica (Shevenell et al., 2011). **(g)** Reconstructed surface air temperature from WAIS Divide deep ice core borehole measurements (Orsi et al., 2012). Thick line shows the mean reconstruction, thin lines the 1σ error; horizontal black line indicates the 1007–2007 C.E. mean. **(h)** WAIS Divide coarse particle percentage (this work) on an inverted axis. Red and blue bars indicate the general time intervals of the MCA and LIA, respectively.

CPD
9, 3125–3174, 2013

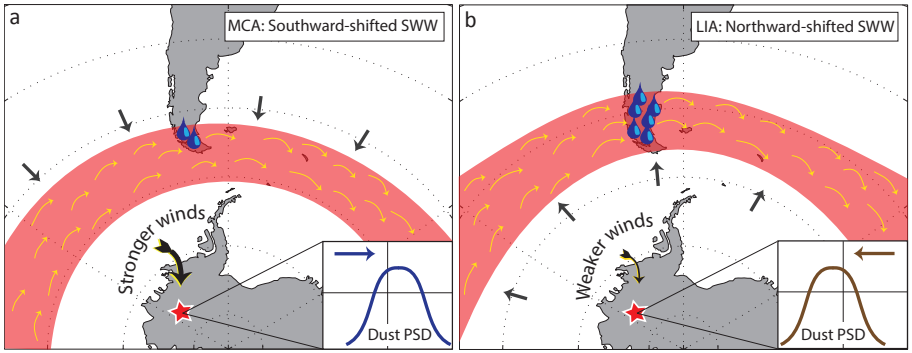

Fig. 9. Schematic diagram showing interpretation of paleoclimate records. **(a)** During the MCA, the SWW are shifted southward, reducing precipitation in the SH mid-latitudes and driving greater cyclogenesis in the Amundsen–Bellingshausen Sea region and stronger winds at the WAIS Divide site, which in turn carry dust with a coarser PSD. **(b)** During the LIA, the SWW are shifted northward, enhancing precipitation in the SH mid-latitudes and reducing cyclogenesis and wind speed in the WAIS Divide region; weaker winds in turn transport dust with a finer PSD.

CPD
9, 3125–3174, 2013

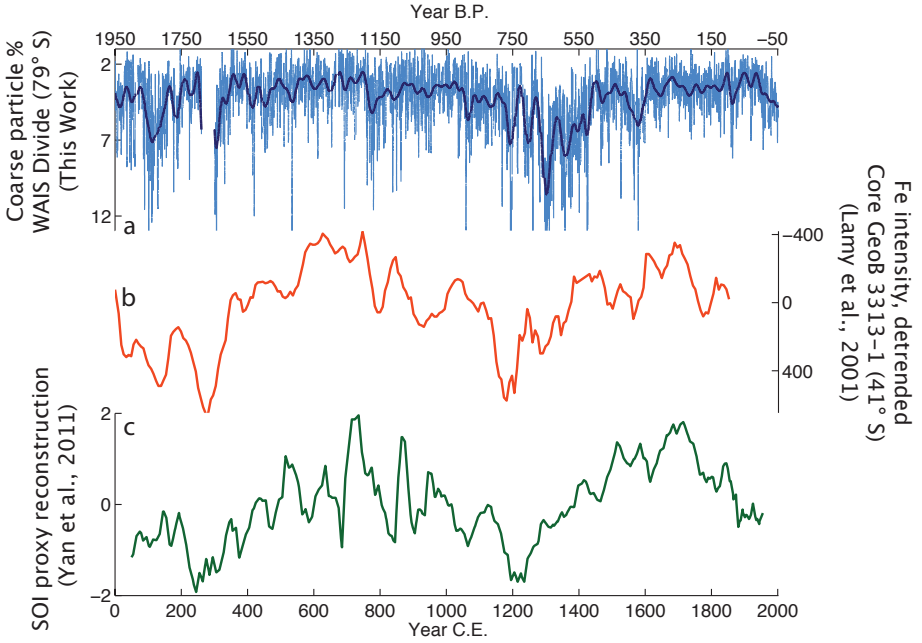

Fig. 10. ENSO and SWW reconstructions: **(a)** WAIS Divide CPP record (this work) on an inverted axis. **(b)** Detrended iron intensity record from marine sediment core GeoB 3313–1 on an inverted axis; low values indicate more humid conditions associated with increased SWW intensity (Lamy et al., 2001). **(c)** Southern Oscillation Index (SOI) precipitation-based reconstruction; negative values indicate a more El Niño-like state (Yan et al., 2011).

CPD
9, 3125–3174, 2013